Journal of
Medicinal Chemistry



Article

# Discovery of Small-Molecule Inhibitors of Receptor Activator of Nuclear Factor-#B Ligand (RANKL) with Superior Therapeutic Index

Vagelis Rinotas, Athanasios Papakyriakou, Foteini Violitzi, Christos Papaneophytou, Maria-Dimitra Ouzouni, Polyxeni Alexiou, Alexandros T. Strongilos, Elias Andreas Couladouros, George A Kontopidis, Elias Eliopoulos, and Eleni Douni

*J. Med. Chem.*, **Just Accepted Manuscript** • DOI: 10.1021/acs.jmedchem.0c01316 • Publication Date (Web): 21 Sep 2020



## Just Accepted



is published by the American Chemical Society. 1155 Sixteenth Street N.W., Washington, DC 20036

# Discovery of Small-Molecule Inhibitors of Receptor Activator of Nuclear Factor-κB Ligand (RANKL) with Superior Therapeutic Index

Vagelis Rinotas,[1,2] Athanasios Papakyriakou,[3] Foteini Violitzi,[2] Christos Papaneophytou,[4,5] Maria-Dimitra Ouzouni,[6] Polyxeni Alexiou,[6] Alexandros Strongilos,[7] Elias Couladouros,[6] George Kontopidis,[4] Elias Eliopoulos,[1] Eleni Douni[1,2,*]

[1]Laboratory of Genetics, Department of Biotechnology, Agricultural University of Athens, 75 Iera Odos, 11855, Athens, Greece
[2]Institute for Bioinnovation, Biomedical Sciences Research Center "Alexander Fleming", 34 Fleming Street, 16672, Vari, Greece
[3]Institute of Biosciences and Applications, National Centre for Scientific Research "Demokritos", 15341, Agia Paraskevi, Athens, Greece
[4]Department of Biochemistry, Veterinary School, University of Thessaly, 224 Trikalon, 43131, Karditsa, Greece
[5]Department of Life and Health Sciences, School of Sciences and Engineering, University of Nicosia, 46 Makedonitissas Avenue, 2417, Nicosia, Cyprus
[6]Laboratory of General Chemistry, Department of Food Science and Human Nutrition, Agricultural University of Athens, 75 Iera Odos, 11855, Athens, Greece
[7]proACTINA SA, 20 Delfon Street, 15125, Marousi-Athens, Greece

[*]Corresponding author: Eleni Douni, Laboratory of Genetics, Department of Biotechnology, Agricultural University of Athens, 75 Iera Odos, 11855, Athens, Greece; douni@aua.gr/ Institute for Bioinnovation, Biomedical Sciences Research Center "Alexander Fleming", 34 Fleming Street, 16672, Vari, Greece; douni@fleming.gr

## ABSTRACT

Receptor activator of nuclear factor-κB ligand (RANKL) constitutes the master mediator of osteoclastogenesis, while its pharmaceutical inhibition by a monoclonal antibody has been approved for the treatment of postmenopausal osteoporosis. To date, the pursuit of pharmacologically more favorable approaches using low-molecular-weight inhibitors has been hampered by low specificity and high toxicity issues. This study aimed to discover small-molecule inhibitors targeting RANKL trimer formation. Through a systematic screening of 39 analogs of SPD-304, a dual inhibitor of TNF and RANKL trimerization, we identified 4 compounds (**1b, 3b, 4a, and 4c**) that selectively inhibited RANKL-induced osteoclastogenesis in a dose-dependent manner, without affecting TNF activity or osteoblast differentiation. Based on structure-activity observations extracted from the most potent and less toxic inhibitors of RANKL-induced osteoclastogenesis, we synthesized a focused set of compounds that revealed 3 potent inhibitors (**19a**, **19b** and **20a**) with remarkably low cell-toxicity and improved therapeutic indexes as shown by the $LC_{50}$ to $IC_{50}$ ratio. These RANKL-selective inhibitors are an excellent starting point for the development of small-molecule therapeutics against osteolytic diseases.

## INTRODUCTION

Bone integrity is maintained through a dynamic process, known as bone remodeling, resulting from a continuous balanced interplay between bone resorption caused by osteoclasts and bone formation employed by osteoblasts. An increase in bone remodeling activity occurs in osteoporosis, the most common bone disease, that is characterized by low bone density, reduced bone quality and increased risk of fractures, causing serious health consequences.[1] Receptor activator of nuclear factor-κB ligand (RANKL), a tumor necrosis factor (TNF) superfamily member, constitutes the master mediator of bone resorption as it promotes osteoclast differentiation, activity and survival.[2–4] It is a type II transmembrane protein that contains a conserved extracellular TNF-like core domain forming an antiparallel β-sheet that is predicted to assemble into homotrimers required for binding to its cognate receptor RANK.[5,6] Trimeric soluble RANKL is also produced either by proteolytic cleavage of the transmembrane form or by alternative splicing.[7,8] Binding of RANKL to RANK initiates downstream signaling cascades, including nuclear factor κB (NF-κB), protein kinases, nuclear factor of activated T-cell c1 (NFATc1) and c-Fos, that activate osteoclastogenic genes.[9] RANKL is also implicated in diverse *in vivo* biological processes such as immune regulation, mammary gland development, hormone-induced breast cancer induction, and body thermoregulation.[10–13] Genetic ablations of RANKL and RANK result in severe autosomal recessive osteopetrosis, a disease caused by osteoclast deficit, demonstrating that the RANKL/RANK system is indispensable for osteoclastogenesis and bone resorption.[14–18] RANKL is physiologically inhibited by the natural decoy receptor osteoprotegerin (OPG) that prevents its binding to the RANK receptor and thus impairs the process of

osteoclastogenesis.[19] An imbalance at the RANKL/OPG ratio caused by abundant RANKL levels is believed to be a major determinant in the development of bone loss diseases, including postmenopausal osteoporosis, bone metastasis, and multiple myeloma.[20,21] Our research group has previously demonstrated that overexpression of human RANKL in transgenic mice leads to progressive bone resorption and osteoporosis in both sexes, establishing unique genetic models of osteoporosis for understanding the underlying pathogenic mechanisms and for preclinical evaluation of novel therapeutics.[22] During the past decades, many anti-osteoporotic therapeutic interventions have been established targeting mainly inhibition of bone resorption and to a lesser extent stimulation of bone formation.[23,24] However, many drawbacks including poor clinical responses, undesired side-effects and high market cost have stimulated the research for new compounds with improved specificity and minimal adverse effects.[25] The discovery of the RANKL/RANK/OPG system offered the possibility of developing novel therapeutics that target specifically the main bone-resorbing factor, RANKL. Denosumab, a human monoclonal antibody to RANKL that specifically blocks its binding to RANK constitutes the first RANKL inhibitor approved by FDA for the treatment of postmenopausal osteoporosis.[26–28] However, functional limitations of therapeutic antibodies have come to light, such as inadequate pharmacokinetics, tissue accessibility and immunogenicity, which point to areas where additional research is needed.[29]

Alternative therapeutic approaches using peptide-mimics,[30,31] natural product inhibitors[32] or small molecules that inhibit RANKL function have been pursued in parallel.[33–37] Inhibition of RANKL using small-molecules has gained considerable attention due to the advantages of their low-cost production, desirable pharmacokinetic properties, and the

potential for oral administration. On these grounds, SPD-304 (Scheme 1) has been previously identified as a potent TNF inhibitor promoting dissociation of trimer assembly[38], which also inhibits RANKL-induced osteoclastogenesis[18,36], whereas its preclinical use has been hampered by its high toxicity.[36,38] SPD-304 contains a potentially toxic 3-alkyindole moiety that can be activated by cytochrome P450 enzymes to produce α,β-unsaturated iminium species.[39] Indeed, toxicological studies have shown that SPD-304 can be dehydrogenated by CYP3A4 to the electrophilic 3-methyleneindolenine intermediate, in addition to other hydroxylation, *N*-dealkylation and epoxidation metabolites.[40] With the aim to develop analogs of SPD-304 with improved toxicity profiles, we have previously employed structure-based design and synthesis of the compounds shown in Scheme 1.[41,42] Their design strategy comprised of: (i) substitution of the trifluoromethylphenyl moiety of SPD-304 with electron-withdrawing groups, such as the phenylsulfonyl or the 3-nitrophenyl groups; (ii) conversion of the diamine linker into the corresponding diamide, or cyclization to 1-4-piperazinylone; and (iii) elimination of the methyl groups of the chromone moiety, or its substitution by other aromatic rings. Their screening against TNF revealed several equally potent inhibitors of TNF with respect to SPD-304,[42] while incorporation of electron-withdrawing substituents at the indole moiety in conjunction with elimination of the 6´-methyl group of the 4-chromone moiety, led to the identification of compound **1c** as a significantly less toxic inhibitor of TNF/TNF-R1.[41]

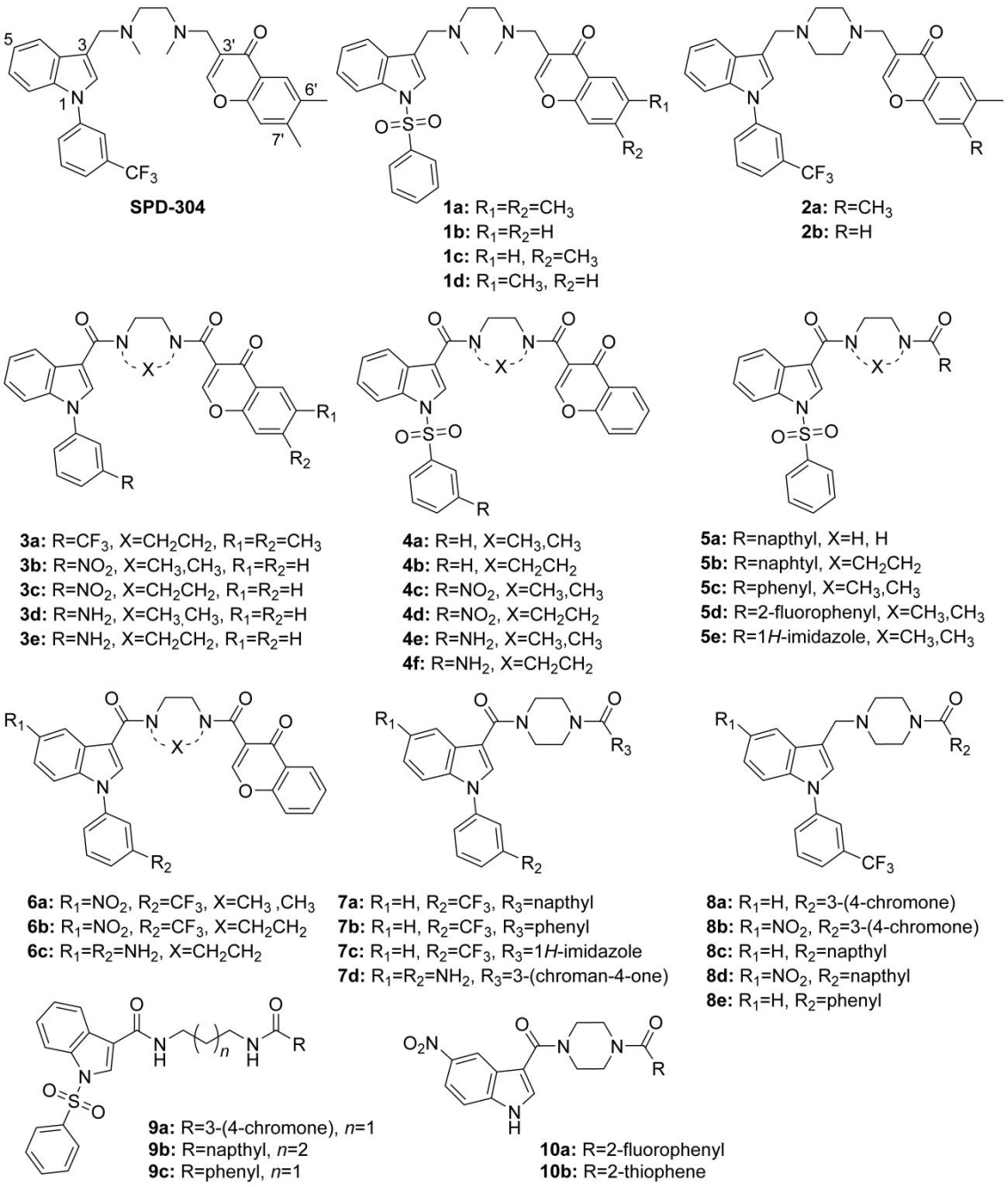


**Scheme 1.** Structures of the compounds designed as TNF inhibitors and used here in a systematic screening against RANKL-induced osteoclastogenesis.

Herein, we report the identification of 7 novel RANKL inhibitors through RANKL-induced osteoclastogenesis assays, further supported by binding affinity and cytotoxicity assays. The efficacy of the compounds and the $IC_{50}$ were estimated through a quantitative RANKL-induced osteoclastogenesis assay, while the MTT assay was used to measure cell viability and the $LC_{50}$ on primary osteoclast precursors stimulated with compounds in a range of concentrations exceeding those tested for their efficacy in the absence of RANKL. By measuring the $LC_{50}$ to $IC_{50}$ ratio (therapeutic index)[43], we evaluated whether the anti-osteoclastogenic effects of the compounds were attributed either to cellular toxicity unrelated to RANKL (ratio close to 1) or specific inhibition of the RANKL function (ratio >>1). Based on the systematic screening of 39 SPD-304 analogs previously screened for TNF inhibition[41,42] (Scheme 1, Table 1), we identified 4 compounds (**1b, 3b, 4a, and 4c**) that displayed total inhibition of RANKL-induced osteoclastogenesis with low toxicity. We also report the development of 3 potent inhibitors (**19a**, **19b**, **20a**) of human RANKL-induced osteoclastogenesis with minimal toxicity in primary cell cultures of osteoclast precursors derived from bone marrow cells. We also suggest their potential binding mode at the interface of human RANKL dimer through ensemble docking calculations using representative structures from a series of molecular dynamics simulations.

**Table 1. List of 39 compounds evaluated as RANKL inhibitors.** With bold are highlighted the 4 most active compounds. [a]Quantification of binding affinity to TNF by fluorescence assay, [b]Mean± SD (n=3 independents experiments); $p<0.01$. [c]Quantification of inhibition of TNF-induced death in L929 cells. [d]Quantification of binding affinity to RANKL by fluorescence assay. [e]Quantification of compounds toxicity in BMM cells. *n.d.*= not determined due to no inhibition of osteoclastogenesis, inactive= no binding affinity, toxic= cell toxicity is observed at 5µM, * *Values taken from* [41,42].

| Compound ID | TNF binding Affinity*[a] ($K_d$, μM)[b] | Inhibition of TNF activity*[c] ($IC_{50}$, μM)[b] | RANKL binding affinity[d] ($K_d$, μM)[b] | Inhibition of osteoclastogenesis at 5 μM | BMM viability[e] ($LC_{50}$, μM) |
|---|---|---|---|---|---|
| **SPD-304** | 5.36 ± 0.21 | 5.00 ± 0.15 | 13.80±0.70 | toxic | <20 |
| **1a** | 8.50±0.56 | 7.50±0.15 | 8.71±0.44 | toxic | *n.d* |
| **1b** | **7.60±0.62** | **50.00 ± 0.11** | **5.24±0.12** | **total** | **>20** |
| **1c** | 5.10±0.23 | 10.00±0.15 | 4.90±0.31 | total | <20 |
| **1d** | 21.00±0.78 | 10.00±0.15 | 6.62±0.27 | toxic | *n.d* |
| **2a** | 10.12 ± 0.67 | 10.00 ± 1.90 | >10 | total | <20 |
| **2b** | 4.78 ± 0.45 | 30.00 ± 3.10 | >11 | none | *n.d* |
| **3a** | 5.12 ± 0.61 | *inactive* | 4.60±0.23 | total | <20 |
| **3b** | **12.22 ± 0.85** | ***inactive*** | **2.18±0.11** | **total** | **>20** |
| **3c** | 25.36 ± 1.25 | *inactive* | >25 | none | *n.d* |
| **3d** | 35.23 ± 1.92 | *inactive* | 17.61±0.78 | none | *n.d* |
| **3e** | 14.12 ± 0.69 | 10.00 ± 1.30 | 19.06±1.47 | none | *n.d* |
| **4a** | **7.00 ± 0.44** | **>60** | **4.60±0.34** | **total** | **>20** |
| **4b** | 12.81 ± 0.78 | 15.00 ± 1.70 | 11.04±0.77 | partial | > 20 |
| **4c** | **3.16 ± 0.21** | **20.00 ± 1.60** | **4.60±0.38** | **total** | **>20** |
| **4d** | 16.82 ± 0.51 | 20.00 ± 2.10 | inactive | total | <20 |
| **4e** | 0.95 ± 0.06 | 25.00 ± 1.80 | 22.30±1.24 | none | *n.d* |
| **4f** | 5.45 ± 0.62 | 20.00 ± 1.90 | *inactive* | none | *n.d* |
| **5a** | >35 | *inactive* | 3.55±0.22 | none | *n.d* |
| **5b** | *inactive* | *inactive* | *inactive* | none | *n.d* |
| **5c** | 17.27 ± 1.26 | *inactive* | >15 | none | *n.d* |
| **5d** | *inactive* | *inactive* | 12.50±0.56 | partial | >20 |
| **5e** | *inactive* | *inactive* | *inactive* | none | *n.d* |
| **6a** | 13.28 ± 1.15 | *inactive* | 2.82±0.31 | total | <20 |
| **6b** | *inactive* | *inactive* | *inactive* | none | *n.d* |
| **6c** | 15.61 ± 1.46 | 40.00 ± 3.80 | 9.31±0.25 | partial | >20 |
| **7a** | *inactive* | *inactive* | *inactive* | none | *n.d* |
| **7b** | 15.17 ± 1.34 | *inactive* | *inactive* | none | *n.d* |
| **7c** | >35 | *inactive* | 5.34±0.41 | partial | <20 |
| **7d** | *inactive* | *inactive* | *inactive* | none | *n.d* |
| **8a** | 1.61 ± 0.15 | 10.00 ± 0.90 | 8.49±0.34 | partial | >20 |
| **8b** | *inactive* | *inactive* | *inactive* | total | <20 |
| **8c** | 7.82 ± 1.06 | 20.00 ± 1.80 | *inactive* | none | *n.d* |
| **8d** | *inactive* | *inactive* | *inactive* | partial | >20 |
| **8e** | 2.11 ± 0.16 | 15.00 ± 1.10 | 18.64±0.63 | partial | >20 |
| **9a** | 5.20 ± 0.65 | 20.00 ± 1.90 | *inactive* | none | *n.d* |
| **9b** | 18.70 ± 1.90 | *inactive* | 18.35±0.95 | none | *n.d* |
| **9c** | *inactive* | *inactive* | *inactive* | none | *n.d* |
| **10a** | 17.85 ± 1.28 | *inactive* | 12.80±0.86 | partial | >20 |
| **10b** | 10.74 ± 1.32 | *inactive* | 15.80±0.64 | none | *n.d* |

## RESULTS AND DISCUSSION

### SPD-304 is a dual inhibitor for TNF and RANKL

SPD-304 (Scheme 1) has been discovered as a potent inhibitor of TNF, which promotes the dissociation of active TNF trimers.[38] A crystallographic structure of TNF in complex with SPD-304 revealed the inhibitor bound at the interface of dimeric TNF intermediate, thus blocking the formation of trimers. To examine whether SPD-304 could also serve as an inhibitor of RANKL we performed a series of biochemical and biological assays. Using an *in vitro* fluorescence binding assay we measured the affinity of SPD-304 for human RANKL, which revealed a dissociation constant ($K_d$ = 13.8 μM) that is higher than the corresponding values reported for TNF ($K_d$ = 5.4 μM).[41] By employing a quantitative osteoclastogenesis assay, we found that SPD-304 is a potent inhibitor of human RANKL-induced osteoclastogenesis in a dose-dependent manner ($IC_{50}$ =1.0 μM, Figure 1A,B).

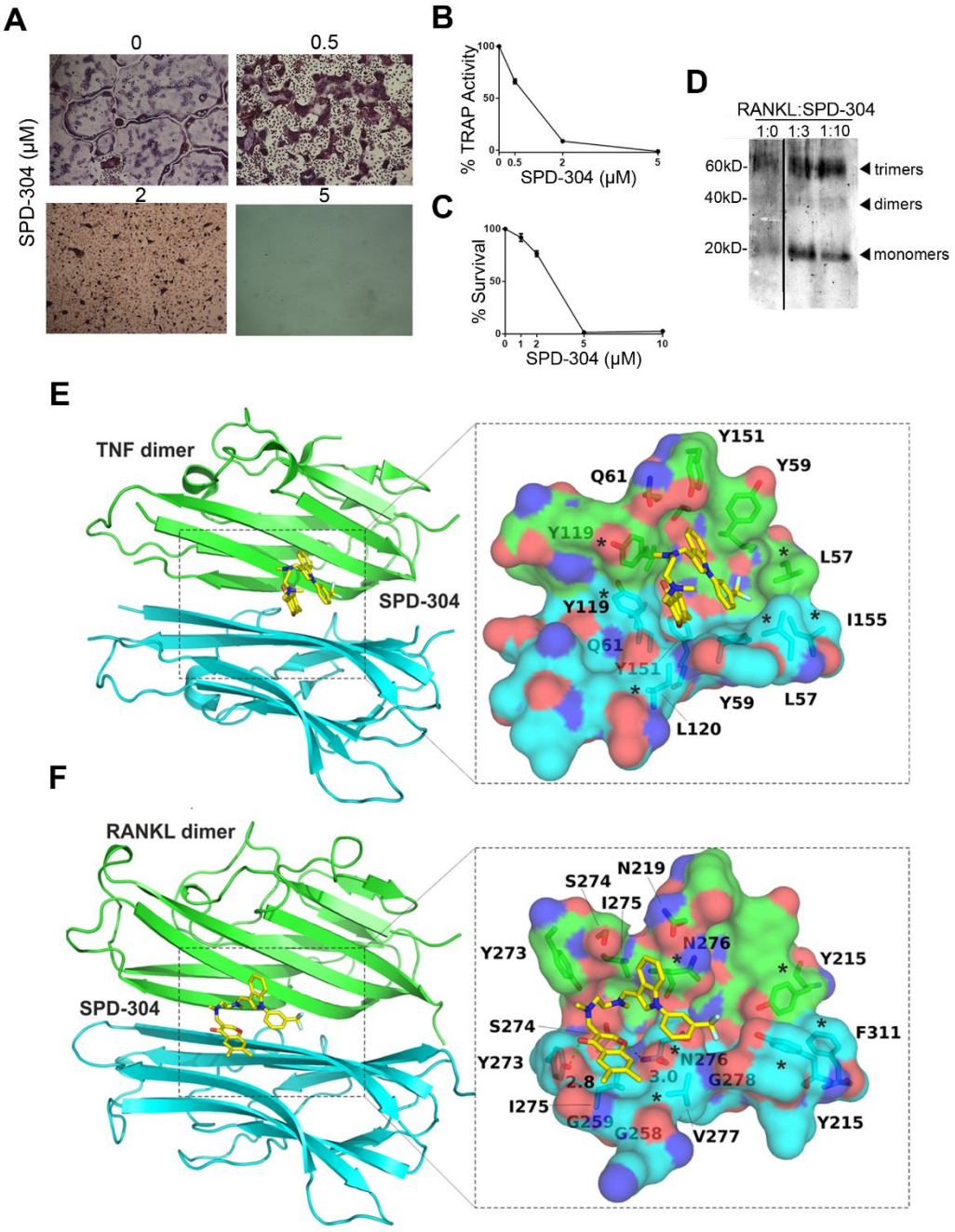


**Figure 1. Functional characterization of SPD-304 as inhibitor of RANKL and molecular modeling of SPD-304 interaction with RANKL.** (**A**) Osteoclastogenesis cultures based on BM cells treated with various concentrations of SPD-304 in the presence of RANKL (40 ng/mL) and M-CSF (25 ng/mL) for 5 days upon staining with TRAP. (**B**) $IC_{50}$ calculation of SPD-304 effect on osteoclastogenesis was based on TRAP activity measured at day 4. (**C**) $LC_{50}$ calculation of SPD304 effect (0-10 μM) on BM cell viability by MTT assay.

(**D**) Recombinant soluble human RANKL and SPD-304 were preincubated and crosslinked with DSS. The crosslinked complex was separated in 12% SDS-PAGE and immunoblotted using an anti-RANKL polyclonal antibody. (**E**) Representation of the X-ray crystal structure of TNF dimer in complex with the small-molecule inhibitor SPD-304 (PDB ID: 2AZ5)[38]. The two TNF subunits are shown in green and cyan for chains A and B, respectively, while the inhibitor is color-coded using yellow C, red O, blue N and cyan F atoms. Inset is a surface representation of the surrounding residues that form the inhibitor-binding pocket, with an asterisk indicating residues that differ in human RANKL. **(F)** Molecular model of human RANKL dimer based on the TNF dimer and the X-ray structure of RANKL complex with the N-terminal fragment of its decoy receptor osteoprotegerin (PDB ID: 3URF).[19] Inset is a close-up view of the RANKL interface, in the same orientation as shown for TNF, illustrating a favorable bound pose of the dual inhibitor SPD-304.

However, SPD-304 proved to be of equally high toxicity to osteoclast precursors derived from bone marrow cells ($LC_{50}$= 3.2 ± 0.1 μM) (Figure 1C, Table 2). To understand the molecular basis of human RANKL inhibition by SPD-304, we investigated its effect at the level of RANKL trimerization using chemical cross-linking experiments. In this experimental setup, pre-incubated soluble human RANKL with SPD-304 at equimolar, or excess molar ratio, were cross-linked and analyzed in SDS polyacrylamide gel electrophoresis (PAGE) for the detection of RANKL trimers, dimers, and monomers. A dramatic increase of RANKL monomers was detected in the presence of SPD-304 (Figure 1D), indicating that the inhibitor promotes human RANKL subunit disassembly. Taken together, we demonstrate that SPD-304 is a dual inhibitor of human TNF and RANKL, which mediates inactivation of the cytokines through dissociation of the

biologically active trimers, but with a low therapeutic index[43] ($LC_{50}$ / $IC_{50}$ = 3.2), indicating high toxicity (Table 2).

**Table 2. Evaluation of potency and toxicity of most effective RANKL inhibitors.** [a]Quantification of inhibition of RANKL-induced TRAP Activity in BM cells, [b]Quantification of compounds toxicity in BMM cells, [c]Values are mean ± standard deviation from 3 independents experiments, [d]Calculated as the ratio of $LC_{50}$ to $IC_{50}$.

| Compound ID | TRAP Activity[a] $IC_{50}$ (µM)[c] | Toxicity[b] $LC_{50}$ (µM)[c] | Therapeutic Index[d] |
|---|---|---|---|
| **SPD-304** | 1.00 ± 0.20 | 3.20 ± 0.10 | 3.2 |
| **1b** | 2.50 ± 0.67 | 58.50 ± 5.00 | 23.4 |
| **3b** | 1.88 ± 0.25 | 44.25 ± 2.64 | 27.8 |
| **4a** | 2.86 ± 1.16 | 62.33 ± 2.59 | 21.8 |
| **4c** | 5.07 ± 0.87 | 32.20 ± 3.55 | 6.3 |
| **19a** | 2.70 ± 0.67 | >300 | >112 |
| **19b** | 2.00 ± 0.19 | >500 | >250 |
| **19c** | 1.90 ± 0.26 | 18.30 ± 1.10 | 9.5 |
| **20a** | 1.40 ± 0.67 | 123.00 ± 4.00 | 84.8 |
| **20b** | 5.10 ± 1.10 | 52.60 ± 7.20 | 10.4 |
| **20c** | 6.40 ± 0.88 | 118.00 ± 26.00 | 18.5 |

## Structural model of RANKL bound to SPD-304

SPD-304 has been shown to bind TNF dimer mostly through a shape-driven interaction within a hydrophobic pocket comprising 6 aromatic tyrosine residues (Tyr59, Tyr119, and Tyr152 from each monomer, Figure 1E). To investigate whether SPD-304 could operate via a similar mechanism as inhibitor of RANKL trimerization, we prepared a model of human RANKL dimer based on the TNF dimer as template and the crystallographic

structure of human RANKL complex with the N-terminal fragment of its decoy receptor OPG.[19] Examination of the model revealed a significant change in the shape of the corresponding pocket at the interface of human RANKL dimer, mainly due to the change of Tyr119 and Leu57 in TNF to Asn276 and Tyr215 in RANKL, respectively (Figure 1F). It is thus reasonable to assume that SPD-304 does not bind RANKL in such a compact conformation as displayed in the co-crystal structure in complex with TNF dimer. Indeed, molecular docking calculations of SPD-304 using the energy minimized model of RANKL dimer revealed a large number of diverse binding modes (clusters of conformations), displaying comparable binding affinities with respect to the standard error of the method (see Computational Methods for more detail). This challenging task was also the case when re-docking of SPD-304 to the X-ray structure of the TNF dimer was performed with the widely-used AutoDock software.[44] In particular, the top-ranked and the most populated clusters of conformations failed to identify the crystallographic bound pose of SPD-304 within a root-mean-square deviation ($RMSD_{ref}$) of 2.5 Å (Supporting Information Table S1 and Figure S1), indicating the large conformational space available on the dimer interface.

To tackle the even more challenging case of human RANKL dimer, for which there is no structural information of small-molecule inhibitors to date, we performed a combination of molecular dynamics simulations (MDs) with docking calculations, a method termed ensemble docking.[45,46] Briefly, a representative set of 5 conformations of human RANKL dimer were extracted from atomistic MDs in explicit solvent using two clustering criteria (Supporting Information Figure S2); one by considering only the interface residues and the second using all residues of the dimer. A characteristic analysis of the MDs revealed

a notable stability of the RANKL dimer model at the 100-ns timescale of the simulations (Supporting Information Figures S3–S4). Docking of SPD-304 at the initial, energy-minimized structure of human RANKL dimer (designated as RANKL-min) and the 5 representative conformations from the MDs (Supporting Information Figure S2) displayed a significant number of low populated clusters of conformations (Supporting Information Table S2). However, including the dynamic structural information using multiple conformations of RANKL allowed for a more systematic selection of the most probable ligand binding mode. Specifically, the highest-populated clusters among the top-10 ranked solutions revealed very similar bound poses of SPD-304 in 5 out of the 6 conformations of RANKL employed (Supporting Information Figure S5). We selected the most populated cluster rather than the highest-ranked conformation for each target considering that this choice has been shown to increase the predictive power of docking in several cases.[47,48] The representative model of RANKL-min in complex with SPD-304 displays the ligand in a significantly different conformation than in the X-ray structure of the TNF dimer (Figure 1E,F), which is accommodated at two shallow pockets separated by Asn276 and flagged by Tyr215 and Tyr273 residues of both RANKL monomers. In this pose, the ligand could form 2 hydrogen bonds between the two chromenone oxygens of SPD-304 as acceptors and the phenolic group of Tyr273 and the main chain amide of Asn276 as donors. Although lack of an experimentally determined structure renders this analysis highly speculative, taken together with our results from the binding assay and the RANKL trimerization cross-linking experiment, suggest a putative mechanism of action similar to that proposed for TNF.[38] Thus, SPD-304 could potentially bind to the

active RANKL trimer in a more extended conformation, forming an intermediate complex that mediates the subunit dissociation process.

**Discovery of 4 selective inhibitors of human RANKL**

The finding that SPD-304 inhibits human RANKL and TNF effectively, prompted us to investigate a series of SPD-304 analogs that have been developed previously as TNF inhibitors (Scheme 1).[41,42] Their systematic screening comprised measurement of their binding affinity for human RANKL in comparison with the reported affinity for TNF,[42] and evaluation of their efficacy to inhibit RANKL-mediated osteoclastogenesis at a single concentration of 5 μM (Table 1). Compounds that displayed partial or total inhibition were further evaluated through MTT viability assay. Analysis of our screening results revealed 10 compounds that completely prevented osteoclast formation and 8 compounds that partially inhibited RANKL-induced osteoclastogenesis. 19 compounds had no effect on RANKL-induced osteoclastogenesis, while 2 compounds displayed similar toxicity to SPD-304 (Table 1). From the 10 most potent RANKL inhibitors (total inhibition of osteoclastogenesis at 5 μM), 4 compounds displayed a relatively low toxicity of $LC_{50}$ >20 μM (**1b**, **3b**, **4a** and **4c**, Scheme 1). Interestingly, these 4 compounds had not been identified as potent inhibitors of TNF activity ($IC_{50} \geq 20$ μM, Table 1), and thus selected for further investigation. Their assessment comprised of osteoclastogenesis assays (quantitative TRAP activity, phalloidin staining), toxicity assays, osteoblast differentiation (alkaline phosphatase activity), RANKL signaling (NFATc1, c-Fos) and RANKL trimerization.

Compound **1b** was developed by substitution of the *m*-trifluoromethylphenyl ring of SPD-304 by a phenylsulfonyl group, in addition to removal of both methyl groups at the 4-chromone moiety (Scheme 1). The binding affinity of **1b** ($K_d$ = 5.24 ± 0.12 μM) displayed a 2.7-fold increase compared to SPD-304 (Table 1). The effect of **1b** on RANKL-induced osteoclastogenesis demonstrated a dramatic inhibition of osteoclast formation at 5 and 10 μM, as shown by the absence of multinuclear TRAP+ cells (Figure 2A), and the decrease of phalloidin-labeled actin ring formation (Figure 2B-C). Further evaluation revealed a RANKL inhibitory potency of $IC_{50}$ = 2.5 μM, with a significantly lower toxicity than SPD-304 ($LC_{50}$= 58.5 ± 5.0 μM for **1b** vs 3.2 ± 0.1 μM for SPD-304) (Figure 2D-E). Cross-linking assays showed that preincubation of **1b** with human RANKL protein promoted a substantial release of monomers in a dose-dependent manner (Figure 2F), suggesting an interference with the RANKL trimerization process. We further investigated whether **1b** mediated undesirable inhibitory effects on osteoblasts. To this scope, we examined the effects of **1b** on the differentiation of pre-osteoblastic MC3T3-E1 cells through quantification of alkaline phosphatase (ALP) activity, a widely recognized marker for osteoblastic differentiation and activity. MC3T3-E1 cells were treated with **1b** at indicated concentrations (Figure 2G) for 14 days and ALP activity was measured at the endpoint. Our analysis showed that **1b** at a concentration range of 2–10 μM did not interfere with osteoblast differentiation and activity (Figure 2G). Therefore, **1b** emerged as a potent RANKL inhibitor with an increased therapeutic index compared to SPD-304 (23.4 vs 3.2, Table 2), indicating low toxicity.

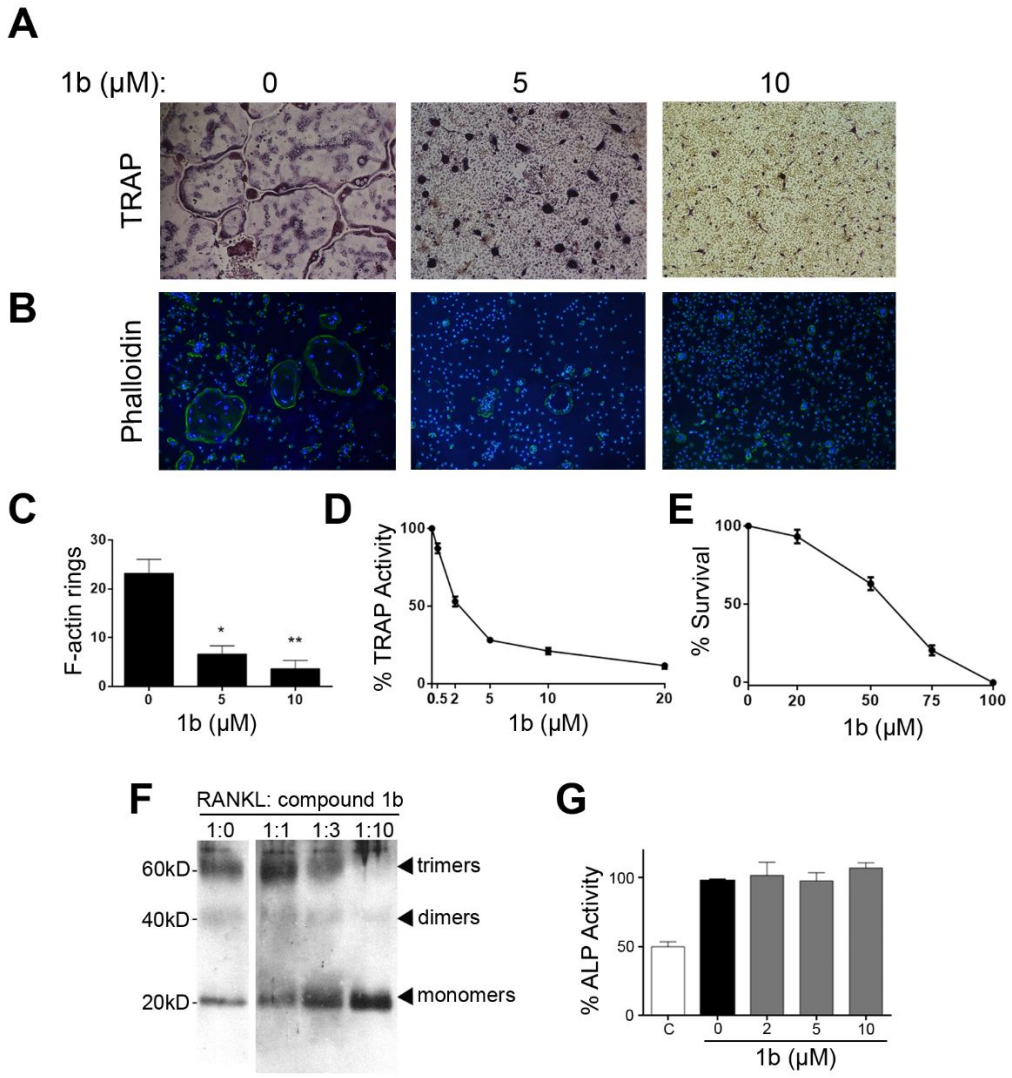


**Figure 2. Characterization of the small-molecule 1b as RANKL inhibitor**. (**A**) Osteoclastogenesis cultures based on BM cells treated with compound **1b** at 5 and 10 μM in the presence of RANKL (40 ng/mL) and M-CSF (25 ng/mL) for 5 days upon staining with TRAP. (**B**) Actin ring organization in osteoclastogenesis cultures upon exposure to compound **1b** at 5 and 10 μM as shown by phalloidin staining (green) and DAPI to visualize nuclei (blue). (**C**) Quantification of intact F-actin rings per $mm^2$ on osteoclastogenesis cultures treated with compound **1b** at 5 and 10 μM. (**D**) $IC_{50}$ calculation for compound **1b** effect on RANKL-induced osteoclastogenesis based on TRAP activity measured at day 4. (**E**) $LC_{50}$ calculation of compound **1b** effect (0–100 μM) on BMM cell viability by MTT assay. (**F**) Recombinant soluble RANKL and compound **1b**

were preincubated either at equal molar ratio or excess and then crosslinked with DSS. The crosslinked complex was separated in 12% SDS-PAGE and immunoblotted using an anti-RANKL polyclonal antibody. (**G**) Effect of compound **1b** (2, 5 and 10 μM) on the differentiation of pre-osteoblastic MC3T3-E1 cells as measured by alkaline phosphatase activity (ALP). Undifferentiated MC3T3-E1 cells are marked as c. All experimental assays were repeated at least three times. Results are presented as means ± SD (n>3). *p>0.05, **p>0.01.

Compound **3b** comprises a diamide linker instead of the diamine moiety in SPD-304, and a 3-nitrophenyl instead of the trifluoromethylphenyl group (Scheme 1). **3b** displayed the highest binding affinity ($K_d$ = 2.18 ± 0.11 μM) among the compounds tested (Table 1), and inhibited RANKL-induced osteoclastogenesis in a dose-dependent manner (Figure 3A-D), as detected by staining of cultures with TRAP and phalloidin, as well as by quantitative TRAP activity ($IC_{50}$ = 1.88 ± 0.25 μM). Regarding cell toxicity, **3b** displayed a superior profile compared to SPD-304 ($LC_{50}$ = 44.25 ± 2.64 μM) (Figure 3E). Moreover, **3b** at a concentration range of 2–10 μM had no effect on MC3T3-E1 differentiation, as measured by ALP activity (Figure 3F). Cross-linking biochemical assays showed that **3b** promoted a dramatic release of human RANKL monomers, even at 1:3 molar ratio (Figure 3G), an effect that is in agreement with the high binding affinity of **3b** for RANKL. We then investigated whether **3b** affects the signaling pathways activated downstream of RANKL by examining the levels of the transcription factors NFATc1 and c-Fos in RAW264.7 cells through western blot.[49–51] Our results indicate that **3b** diminished the NFATc1 and c-Fos protein levels in RAW264.7 cells treated with RANKL (Figure 3H). Taken together, these data indicate that **3b** promotes inhibition of RANKL-induced osteoclastogenesis and as

a consequence of RANKL-induced signaling pathways involving NFATc1 and c-Fos, while its toxicity is much lower than SPD-304 based on the therapeutic index (27.8 vs 3.2, Table 2).

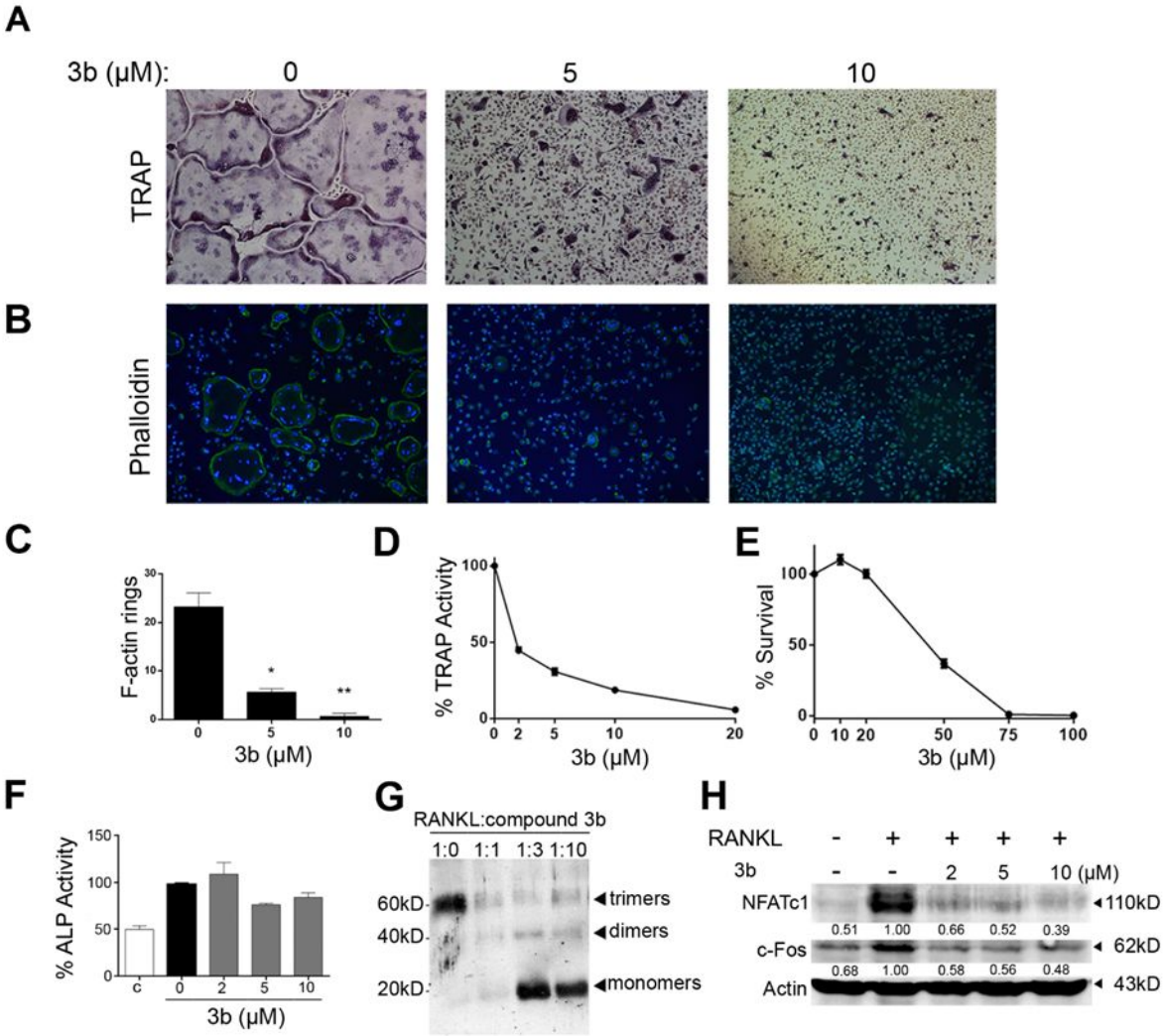


**Figure 3. Characterization of the small-molecule 3b as RANKL inhibitor**. (**A**) Osteoclastogenesis cultures treated with compound **3b** at 5 and 10 μM in the presence of RANKL (40 ng/mL) and M-CSF (25 ng/mL) for 5 days upon staining with TRAP. (**B**) Actin ring organization in osteoclastogenesis cultures upon exposure to compound **3b** at 5 and 10 μM as shown by phalloidin staining and DAPI. (**C**) Quantification of intact F-actin rings per $mm^2$ on osteoclastogenesis cultures treated with compound **3b** at 5 and

10 μM. (**D**) $IC_{50}$ calculation for compound **3b** effect on RANKL-induced osteoclastogenesis based on TRAP activity measured at day 4. (**E**) $LC_{50}$ calculation of compound **3b** effect (0–100 μM) on BMM cell viability by MTT assay. (**F**) Effect of compound **3b** (2, 5 and 10 μM) on the differentiation of pre-osteoblastic MC3T3-E1 cells as measured by ALP activity. (**G**) Recombinant soluble RANKL and compound **3b** were preincubated either at equal molar ratio or excess and then crosslinked with DSS. The crosslinked complex was separated in 12% SDS-PAGE and immunoblotted using an anti-RANKL polyclonal antibody. (**H**) Western blot showing the effect of preincubated compound **3b** with RANKL at the indicated concentrations on the induction of NFATc1 and c-Fos in RAW264.7 cells. Antibody specific for β-actin was used for normalization. Numbers below NFATc1 and c-Fos blots indicate relative expression compared to positive control. All experimental assays were repeated at least three times. Results are presented as means ± SD (n>3). *$p$>0.05, **$p$>0.01.

Compound **4a** is the closest analog of **1b**, but with diamide moiety as in **3b** (Scheme 1). Biochemical evaluation revealed that **4a** displayed a 3-fold higher binding affinity than SPD-304 (Table 1), and effectively inhibited osteoclastogenesis in a dose-depended manner ($IC_{50}$ = 2.86 ± 1.16 μM, Supporting Information Figure S6A-D). More importantly, **4a** was found to be 20-fold less toxic than SPD-304 ($LC_{50}$ = 62.33 ± 2.59 μM), without affecting differentiation of the pre-osteoblastic cell line MC3T3-E1 (Supporting Information Figure S6E,F).

The fourth potent inhibitor identified, **4c,** is a 3-nitrophenylsulfonyl derivative of **4a** (Scheme 1). Similarly, **4c** showed an improved binding affinity with respect to SPD-304 ($K_d$ = 4.60 ± 0.38 μM), displayed inhibition of osteoclast formation in a dose-dependent manner ($IC_{50}$ = 5.07 ± 0.87 μM, Supporting Information Figure S7A-D), with a 10-fold lower cell-toxicity compared to SPD-304 ($LC_{50}$ = 32.20 ± 3.55 μM, Supporting Information

Figure S7E). **4c** also effectively reduced the induction of the transcription factors NFATc1 and c-Fos in RAW264.7 cells, while not affecting differentiation of pre-osteoblastic cells (Supporting Information Figures S7F,G), indicating a specific effect of **4c** in RANKL-induced osteoclastogenesis. Taken together, compounds **1b**, **3b**, **4a** and **4c** inhibit RANKL-induced osteoclastogenesis and display an increase of the therapeutic index, 2-8 times compared to SPD-304 (Table 2).

**Structure-activity relationships of the identified RANKL inhibitors**

Considering the structural characteristic of the 4 most potent and less toxic inhibitors identified, we can make the following observations. With respect to the parent compound (SPD-304) all 4 potent inhibitors of RANKL comprise the 4-chromone moiety but without its two methyl substituents. In 3 of these (**1b**, **4a** and **4c**) the trifluoromethylphenyl group is replaced by a phenylsulfonyl moiety, whereas **3b** contains the 3-nitrophenyl moiety. Interestingly, although the nitro group is considered as a toxicophore, albeit its wide use in therapeutics,[52] 2 out of the 4 RANKL inhibitors (**3b** and **4c**) contain the 3-nitrophenyl moiety and are >10-fold less toxic than SPD-304. Lastly, except for **1b** that comprise the diamine linker as in SPD-304, this moiety is converted to the more rigid diamide in the other 3 inhibitors. To gain further insight into their structure-activity relationships, we predicted their binding mode to human RANKL dimer following the same methodology as described above (Figure 4). As in the case of SPD-304, the docking results were evaluated by means of the most populated clusters of conformations in the 6 representative structures of the RANKL dimer (Supporting Information Tables S3–S6 and Figures S8–S10). Specifically, the most favorable bound pose of **1a** was selected in conjunction with those displayed by **4a**, similarly to the selection of the most favorable

conformations for **3b** and **4c**. For the first couple of inhibitors (Figure 4A,C), the presence of the phenylsulfonyl-1*H*-indole moiety favors its interaction at an aromatic-rich pocket comprising of Tyr215 (both chains A and B), Tyr217(B) and Tyr307(B). In this bound pose, their sulfonyl group can accept 2 hydrogen bonds from the side-chain amide of Asn276(B) and the phenolic group of Tyr215(B). Although conversion of the diamine of **1b** to diamide in **4a** decrease its conformational freedom, the linker with the 4-chromone moiety is accommodated accordingly to accept a hydrogen bond from the main chain amide of Asn276(A) and probably interact with Gly278(A) as well (Figure 4A,C). For inhibitors **3b** and **4c**, it is possible that the presence of the nitro group can mediate their binding at an inverted orientation with respect to **1b** and **4a** (Figure 4B,D). This effect is probably due to the favorable hydrogen-bonding interactions with the two side chain amines of Lys262 (chains A and B), in addition to a potential hydrogen bond with the phenolic group of Tyr273(A). The sulfonyl group of **4c** display the potential to form hydrogen bonds with the hydroxyl groups of Tyr273(B) and probably Ser274(A), which are not possible for **3b** (Figure 4B), which in contrast, exhibits the potential to form a hydrogen bond with the main-chain amide of Asn276(B) (Figure 4D). For both **3b** and **4c**, the 4-chromone moiety is predicted to interact with Tyr215 (both A and B) without exhibiting any hydrogen bonds, whereas the adjacent carbonyl group of their linker can form a hydrogen bond with the amide of Gly278(A).

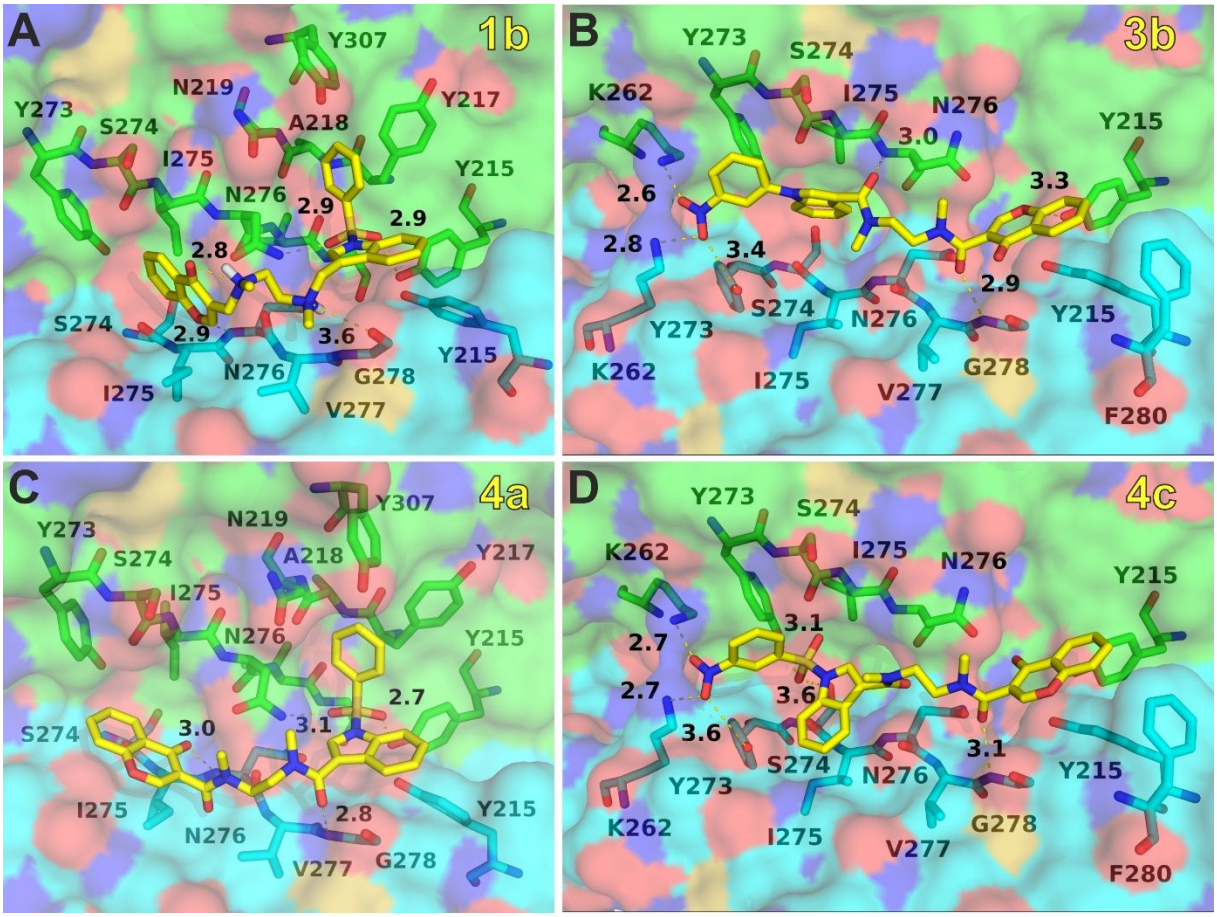


**Figure 4. Close-up view of human RANKL dimer models in complex with the 4 potent inhibitors 1b (A), 3b (B), 4a (C) and 4c (D)**. Putative hydrogen bonding interactions are indicated with yellow dashed lines and the heavy atom distance in Å, whereas atom colors are as described in Figure 1. The models of RANKL dimer were based on the X-ray structure of human RANKL with PDB ID: 3URF.[19]

**Development of 3 potent inhibitors of RANKL-induced osteoclastogenesis with low cell-toxicity**

Based on the above observations, we decided to investigate the effect of substituting the 4-chromone and its adjacent amide moiety with a phenylsulfonylamide group. Although substitution of the 4-chomone ring of SPD-304 by other aryl or heteroaryl rings (e.g. **5a-e**, **7a-d**, **8c-e**, **9b-c** and **10a-b** in Scheme 1) did not reveal any potent inhibitor of RANKL, rather than partial inhibitors of osteoclastogenesis (**7c**, **8d-e** and **10a** in Table 1), our choice was mainly driven by the positive effect of the phenylsuflonyl group displayed by the most potent inhibitors **1b**, **4a** and **4c**. By considering the potential hydrogen bonding interactions of the 3-nitrophenyl group of **4c** (Figure 4D), we prepared compounds **19a-c** according to Scheme 2.

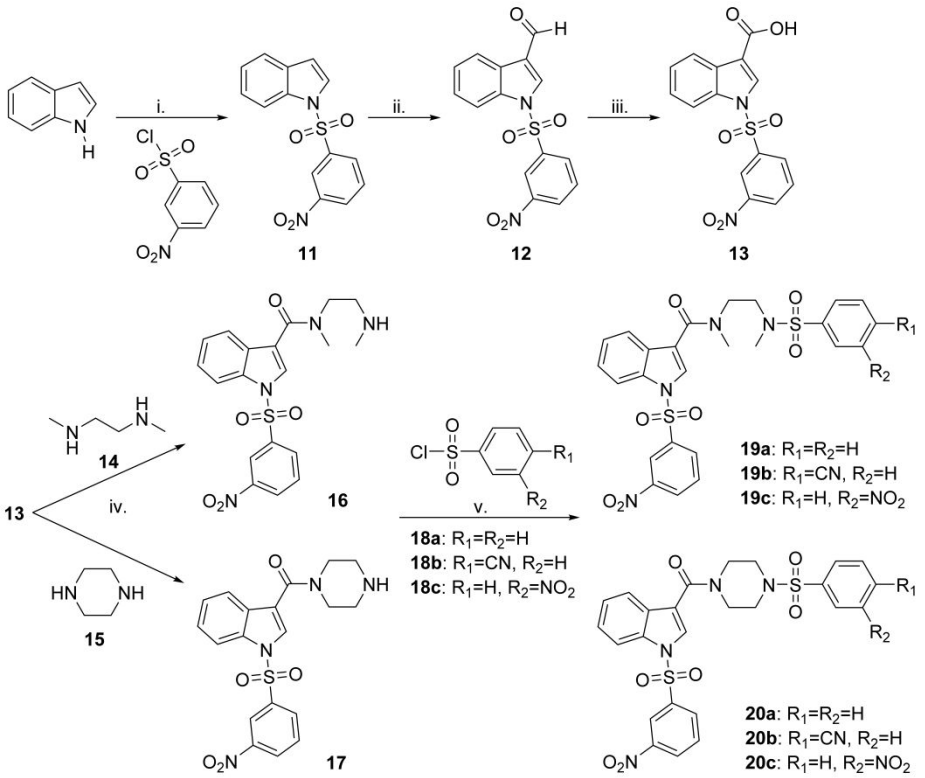

**Scheme 2.** Synthesis of compounds **19a-c** and **20a-c**.Reagents and conditions: (i) KOH, EtOH; then acetone at r.t.; (ii) $POCl_3$, DMF at r.t; then aq. KOH reflux; (iii) $NaClO_2$, $H_3NSO_3$, *t*-BuOH/$H_2O$ at r.t.; (iv) $C_6F_5OH$, EDC, DCM at r.t.; (v) $Et_3N$, DCM at r.t.

In particular, the 4-chromone ring and the adjacent amide of **4c** have been substituted by phenylsulfonylamide (**19a**), 4-cyano-phenylsulfonylamide (**19b**) and 3-nitro-phenylsulfonylamide (**19c**). We also prepared the corresponding cyclized piperazine derivatives **20a**, **20b**, and **20c** (Scheme 2), with the aim to investigate the effect of the additional conformational restriction imposed by the cyclization of the linker moiety, and based on the results obtained for the cyclized analogs of two potent RANKL inhibitors. Specifically, **4b** and **4d** (the piperazine analogs of **4a** and **4c**, Scheme 1) displayed partial and total inhibition of osteoclastogenesis, but with low and high toxicity, respectively (Table 1).

Experimentally, all 6 compounds effectively inhibited RANKL-induced osteoclast formation within an $IC_{50}$ range of 1.40–6.40 μM and were less toxic than SPD-304 (Figure 5A-C, Supporting Information Figure S11, Table 2). Notably, three compounds (**19a**, **19b**, and **20a**) displayed an increase of the therapeutic index ($LC_{50}$/ $IC_{50}$ ratio), more than 25 times compared to SPD-304 (Table 2). In particular, **19a** and **19b** displayed a dramatic decrease of cellular toxicity, exhibiting $LC_{50}$ values of more than 300 and 500 μM, respectively, while retaining a high inhibitory effect in RANKL-induced osteoclastogenesis. Compound **20a** displayed the lowest $IC_{50}$ values in TRAP activity and attenuated NFATc1 and c-Fos induction upon RANKL treatment with a significant (40-fold) decrease in toxicity with respect to SPD-304 (Figure 5D, Table 2). On the other hand, **19c**, **20b** and **20c** displayed a mild increase of the therapeutic index ($LC_{50}$/ $IC_{50}$

ratio), 3-6 times compared to SPD-304 (Table 2). Taken together our results indicate that despite the small number of compounds tested, we succeeded in developing 3 new inhibitors of RANKL-induced osteoclastogenesis with a high therapeutic index ($LC_{50}$ / $IC_{50}$ > 85).

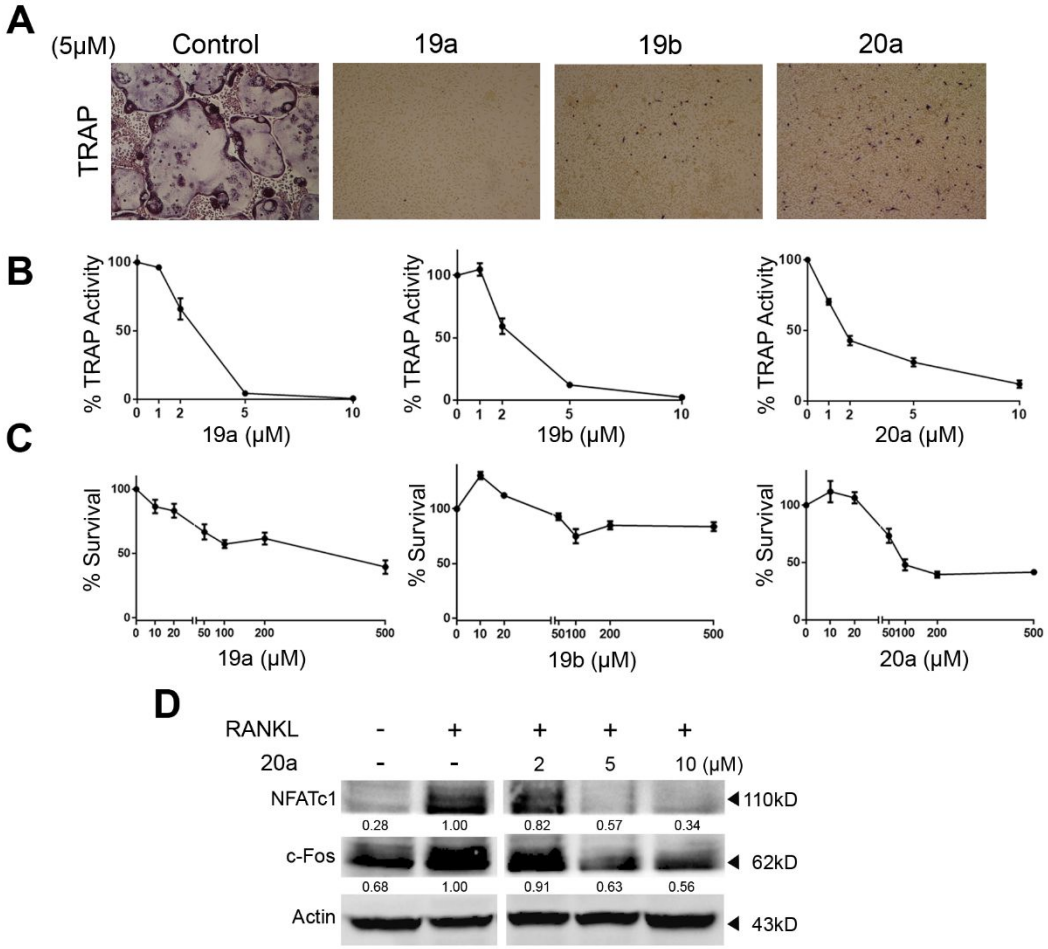


**Figure 5. Compounds 19a**, **19b and 20a inhibit human RANKL-induced osteoclastogenesis and exhibit a dramatic decrease of toxicity**. (**A**) Osteoclastogenesis cultures treated with compounds **19a**, **19b** and **20a** at 5μM in the presence of RANKL (40 ng/mL) and M-CSF (25 ng/mL) for 5 days upon staining with

TRAP. (**B**) $IC_{50}$ calculation for each compound effect on RANKL-induced osteoclastogenesis based on TRAP activity measured at day 4. (**C**) $LC_{50}$ calculation for each compound on BMM cell viability by MTT assay. (**D**) Western blot showing the effect of preincubated compound **20a** with RANKL at the indicated concentrations on the induction of NFATc1 and c-Fos in RAW264.7 cells. All experimental assays were repeated at least three times.

Examination of the molecular models of the most potent compounds (Supporting Information Tables S7–S9 and Figures S12–S13) reveals that introduction of the second phenylsulfonyl moiety in **19a** and **19b**, the 2 less toxic compounds identified (Figure 6), retains the overall binding geometry with respect to that predicted for **3b** and **4c** (Figure 4). However, the increased versatility of the phenylsulfonyl group with respect to the rigid chromenone ring exhibits a potential to be accommodated inside the shallow pocket of RANKL, in addition to the formation of a putative hydrogen bond with the side chain of Tyr215(A). The 4-cyano substituent of **19b** shows an additional hydrogen bonding potential as acceptor from the phenolic group of Tyr307(A) at the base of the pocket (Figure 6B). Notably, the selected model of a cyclized analog, **20a**, revealed a very similar mode of binding with **19a-b** (Figure 6C), albeit the conformational restraint imposed by the 1,4-substituted piperazine moiety. Still, however, experimental verification of these predictions has to wait for the determination of a co-crystal structure with the human RANKL dimer.

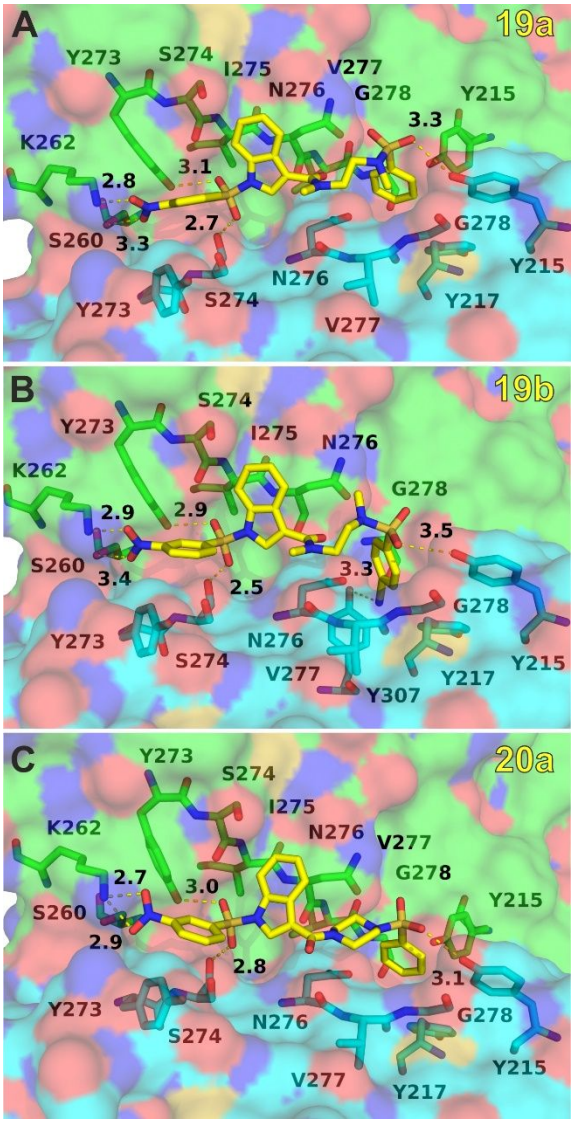


**Figure 6. Close-up views of the predicted inhibitor binding interface RANKL in complex with 19a (A), 19b (B), and 20a (C).** Putative hydrogen bonding interactions are indicated with yellow dashed lines and the heavy atom distance in Å, whereas atom colors are as described in Figure 1. The models of RANKL dimer were based on the X-ray structure of human RANKL with PDB ID: 3URF.[19]

## CONCLUSION

The development of RANKL inhibitors constitutes the most efficient approach to treat osteoporosis and other bone resorption diseases. To date, the monoclonal antibody denosumab has been approved for postmenopausal osteoporosis and bone metastasis from solid tumors[26–28], while only a few selective small-molecule inhibitors of RANKL have been identified as alternative therapeutics[36,37]. Unfortunately, the majority of the potential RANKL inhibitors were screened in activity and viability cell assays at similar concentration ranges without providing $IC_{50}$ and $LC_{50}$ values, arising concerns about interference of toxicity with the observed effectiveness.[37,53] Furthermore, the use of immortalized cell lines such as the preosteoclastic RAW264.7 cells for the $LC_{50}$ evaluation[35,53,54] could lead to underestimation of the compound toxicity compared to primary cell cultures. Thus, the therapeutic index ($LC_{50}$ to $IC_{50}$ ratio) is an important indicator of the probability of the successful development of a drug. SPD-304, despite its promising effect as a dual inhibitor of RANKL and TNF[41,42], displays a low therapeutic index ($LC_{50}$ / $IC_{50}$ = 3.2), indicating high toxicity.

In the present study, we evaluated systematically 39 compounds against human RANKL, using quantitative biochemical and cellular assays based on primary pre-osteoclasts to determine their binding affinity, inhibition potency and toxicity, including specific cellular assays to elucidate their mechanism of action. Four compounds, **1b**, **3b, 4a**, and **4c**, exhibited a dose-dependent inhibition of RANKL-induced osteoclastogenesis and displayed substantially lower toxicity compared to SPD-304 ($LC_{50}$/$IC_{50}$ range between 6.3 and 27.8). At the mechanistic basis of inhibition, we demonstrated that compounds **1b** and **3b** interfered with the trimerization of human RANKL protein, similarly to SPD-304.

At the signaling cascade level, selected compounds (**3b**, **4c**) ameliorated RANKL signaling through the reduction of NFATc1 and c-Fos induction upon RANKL stimulation. More importantly, these 4 inhibitors displayed high selectivity for RANKL-induced osteoclastogenesis, without any observable inhibition of TNF activity, or osteoblast differentiation. Based on these findings we synthesized and evaluated a focused set of compounds, which revealed 3 more potent inhibitors (**19a**, **19b** and **20a**). Interestingly, these compounds exhibited the lowest toxicity among the compounds tested, revealing high therapeutic indexes with $LC_{50}/IC_{50}$ ratios from 85 to more than 250.

Taken together, our systematic study revealed 7 inhibitors of RANKL-induced osteoclastogenesis that display low toxicity, 3 of which with a dramatic increase of the therapeutic indexes, that can be used as a starting point for the development of safe small molecule-based therapeutic approaches in osteolytic diseases.

# EXPERIMENTAL SECTION

## Materials

All final compounds were purified to ≥95% purity as determined by the liquid chromatography–mass spectrometry (LCMS) system described below. LCMS data was collected on a Shimadzu LCMS system equipped with a DGU-20A3 degasser, an LC-20AD binary gradient pump, an SPD-20A photodiode array detector, an SIL-20AC autosampler, a CTO-20AC column oven, an LCMS-2010EV single quadrupole mass spectrometer, and a Purospher RP8 250 × 4.6 mm × 5.0 µm column using Formic acid in aqueous $CH_3COONH_4$ 10 mM to adjust pH=3.9 (A) and LCMS-grade Methanol (B) at a flow rate of 0.5 mL/min and a run time of 45.01 min. The gradient profiles were 80% B to 100% B in 20 min, held for 15 min, at 35.01 min 80% B, held until 45.01 min. Max plot conditions: the wavelength was set at 225 and 254 nm. Purity is reported as the lowest value peak area. NMR spectra were recorded on a Bruker Advance spectrometer operating at 500 MHz for proton ($^1$H NMR) and 126 MHz for carbon ($^{13}$C NMR); chemical shifts are reported in ppm (δ) relative to residual protons in deuterated solvent peaks. Molecular formula and SMILES strings of all compounds tested are provided in the Supporting Information.

## Synthetic route for compounds 19a-c, 20a-c

**1-((3-nitrophenyl)sulfonyl)-1*H*-indole (11).** Commercially available 1*H*-indole (1.0 mmol) was added in a solution of potassium hydroxide (1.2 mmol) in ethanol (10 mL) and the reaction mixture remained under stirring for 10 min at room temperature. Then ethanol was removed under reduced pressure and acetone (10 mL) was added as solvent media. After 5 min, 3-nitrobenzenesulfonyl chloride (1.2 mmol) was added

dropwise and the reaction mixtures remained for 3 h under stirring. The formed solid was removed by filtration and the corresponding filtrate was condensed under reduced pressure. The remained residue was washed with cold ethanol (3×10 mL), dried and further purified with flash column chromatography.

**1-((3-nitrophenyl)sulfonyl)-1*H*-indole-3-carbaldehyde (12).** In an ice bath phosphoryl chloride ($POCl_3$) (2.5 mmol) was added dropwise in dimethylformamide (DMF) (5 mL per 1 mL $POCl_3$). The reaction mixture was stirred for 5 min and then **11** (1 mmol) was added as a solution in dimethylformamide (DMF) (10 mL per 1 g of **11**). The reaction mixture was left under stirring at room temperature for 3 h. After completion of the reaction, 10 mM from aqueous KOH 3.8 M was added dropwise and the reaction mixture was left to reflux overnight. After cooling at room temperature, saturated sodium bicarbonate ($NaHCO_3$) was added. The aqueous phase was washed with ethyl acetate (EtOAc) (3×10 mL), the organic phases were collected, dried over sodium sulfate ($Na_2SO_4$) and condensed under reduced pressure. Aldehyde **12** was used in the next step without further purification.

**1-((3-nitrophenyl)sulfonyl)-1*H*-indole-3-carboxylic acid (13).** Sodium chlorite ($NaClO_2$, 2 mmol) and sulfamic acid ($H_3NSO_3$, 6 mmol) were added in a solution of **12** in *tert*-butanol/$H_2O$ (20 mL, 1:1) at room temperature and the reaction mixture was stirred for 2 h. After completion of the reaction ethyl acetate (20 mL) was added and the organic phase was washed with 0.1 N HCl (1×10 mL), $H_2O$ (4×10 mL) και NaCl (2×5 mL). The organic phase was dried over sodium sulfate ($Na_2SO_4$) and condensed under reduced pressure. The resulting residue was treated with cold ether and was further purified with flash column chromatography.

***N*-methyl-*N*-(2-(methylamino)ethyl)-1-((3-nitrophenyl)sulfonyl)-1*H*-indole-3-carboxamide (16)** and **(1-((3-nitrophenyl)sulfonyl)-1*H*-indol-3-yl)(piperazin-1-yl)methanone (17).** Pentafluorophenol (2.2 mmol) and 1-Ethyl-3-(3-dimethylaminopropyl) carbodiimide (EDC, 2.2 mmol) was added to a solution of **13** (1.0 mmol) in dichloromethane (DCM, 12 mL) at 0 ºC. The reaction mixture was stirred for 4 h at room temperature. Then DCM was removed under reduced pressure and the formed residue was dissolved in chloroform, cooled at 0 ºC and a solution of amine **14** or **15** (10 mmol) in chloroform ($CHCl_3$, 10 mL) was added. The reaction mixture was left under stirring at room temperature for 12 h. The white solid formed was removed from the reaction mixture via filtration and the filtrate was washed with water (3×10 mL). The organic phase was dried over sodium sulfate ($Na_2SO_4$) and condensed under reduced pressure. The resulting residue was further purified with flash column chromatography to produce the corresponding amine **16** or **17**, respectively.

**General procedure for the preparation of 19a-c and 20a-c.** To a solution of the amine **16** or **17** (1.0 mmol) in dichloromethane (DCM, 6 mL), triethylamine ($Et_3N$, 22 mmol), the corresponding sulfonyl chloride **18a-c** (1.5 mmol) was added and the reaction mixture was stirred at room temperature for 3 h. After completion of the reaction DCM was added and the organic phase was washed with water (3×10 mL), dried over sodium sulfate ($Na_2SO_4$) and condensed under reduced pressure. The resulting residue was further purified with flash column chromatography to produce the corresponding final compounds **19a-c** and **20a-c** (Scheme 2) in good yields. Their $^1H$ and $^{13}C$ NMR spectra, and the LCMS analysis are provided in the Supporting Information Figures S14−S19.

***N*-methyl-*N*-(2-(*N*-methylphenylsulfonamido)ethyl)-1-((3-nitrophenyl)sulfonyl)-1*H*-indole-3-carboxamide (19a)**. Yield: 66.4% (purity: 100.0%). $[M+H]^+$: $C_{25}H_{25}N_4O_7S_2^+$; Calc. Mass, $[M+H]^+$: 557.12; Found mass, $[M+H]^+$: 557.35; $^1H$ NMR (500 MHz, $CDCl_3$) δ 8.79 (s, 1H), 8.38 (d, *J* = 7.6 Hz, 1H), 8.22 (bs, 1H), 8.02 (d, *J* = 8.3 Hz, 1H), 7.87 (s, 1H), 7.78 (bs, 3H), 7.68 (t, *J* = 8.1 Hz, 1H), 7.60 (t, *J* = 7.3 Hz, 1H), 7.53 (t, *J* = 7.3 Hz, 2H), 7.41 (t, *J* = 7.7 Hz, 1H), 7.34 (t, *J* = 7.6 Hz, 1H), 3.77 (s, 2H), 3.31 (s, 2H), 3.23 (s, 3H), 2.83 (s, 3H). $^{13}C$ NMR (125.5 MHz, $CDCl_3$) δ 165.39, 148.34, 139.63, 134.44, 132.91, 132.81, 132.61, 131.29, 129.34, 129.09, 128.71, 127.31, 126.62, 126.51, 126.47, 126.16, 124.91, 122.40, 122.27, 122.09, 113.35, 47.68, 45.23, 38.09, 35.40.

***N*-(2-((4-cyano-*N*-methylphenyl)sulfonamido)ethyl)-*N*-methyl-1-((3-nitrophenyl)sulfonyl)-1*H*-indole-3-carboxamide (19b)**. Yield: 67.0% (purity: 94.6%); $[M+H]^+$: $C_{26}H_{24}N_5O_7S_2^+$; Calc. Mass, $[M+H]^+$: 582.11; Found mass, $[M+H]^+$: 582.20; $^1H$ NMR (500 MHz, $CDCl_3$) δ 8.76 (s, 1H), 8.38 (d, *J* = 7.9 1H), 7.67 (t, *J* = 8.0 Hz, 1H), 7.41 (t, *J* = 7.5 Hz, 1H), 7.33 (t, *J* = 7.5 Hz, 1H), 3.78 (s, 2H), 3.36 (s, 2H), 3.24 (s, 3H), 2.87 (s, 3H). $^{13}C$ NMR (125.5 MHz, $CDCl_3$) δ 165.52, 148.39, 139.56, 134.43, 133.18, 132.48, 131.22, 129.00, 128.74, 127.86, 126.58, 126.21, 124.92, 122.43, 122.00, 118.44, 117.32, 116.64, 113.37, 47.66, 45.22, 38.14, 35.28.

***N*-methyl-*N*-(2-((*N*-methyl-3-nitrophenyl)sulfonamido)ethyl)-1-((3-nitrophenyl)sulfonyl)-1*H*-indole-3-carboxamide (19c)**. Yield: 51.7% (purity: 100.0%); $[M+H]^+$: $C_{25}H_{24}N_5O_9S_2^+$; Calc. Mass, $[M+H]^+$: 602.1; Found mass, $[M+H]^+$: 602.25; $^1H$ NMR (500 MHz, $CDCl_3$) δ 8.78 (s, 1H), 8.61 (s, 1H), 8.45 (d, *J* = 8.1 Hz, 1H), 8.39 (d, *J* = 8.1 Hz, 1H), 8.22 (d, *J* = 7.2 Hz, 1H), 8.12 (s, 1H), 8.02 (d, *J* = 8.3 Hz, 1H), 7.87 (s, 1H), 7.77 (t, *J* = 7.8 Hz, 2H), 7.68 (t, *J* = 8.1 Hz, 1H), 7.42 (t, *J* = 7.7 Hz, 1H), 7.34 (t, *J* = 7.6

Hz, 1H), 3.81 (s, 2H), 3.40 (s, 2H), 3.26 (s, 3H), 2.91 (s, 3H). $^{13}$C NMR (125.5 MHz, $CDCl_3$) δ 165.49, 148.60, 148.43, 140.31, 139.63, 134.49, 132.82, 132.51, 131.25, 130.82, 129.09, 128.76, 127.36, 126.56, 126.24, 124.96, 122.48, 122.30, 122.06, 118.52, 113.40, 47.72, 45.12, 38.10, 35.33.

**(1-((3-nitrophenyl)sulfonyl)-1*H*-indol-3-yl)(4-(phenylsulfonyl)piperazin-1-yl)methanone (20a).** Yield: 79.0% (purity: 99.8%); $[M+H]^+$: $C_{25}H_{23}N_4O_7S_2^+$; Calc. Mass, $[M+H]^+$: 555.1; Found mass, $[M+H]^+$: 555.35; $^1$H NMR (500 MHz, $CDCl_3$) δ 8.73 (t, *J* = 1.8 Hz, 1H), 8.42 (dd, *J* = 8.2, 1.1 Hz, 1H), 8.19 (d, *J* = 8.0 Hz, 1H), 7.99 (d, *J* = 8.4 Hz, 1H), 7.76 (d, *J* = 7.2 Hz, 2H), 7.73-7.62 (m, 2H), 7.61 – 7.49 (m, 2H), 7.45-7.28 (m, 4H), 3.78 (s, 4H), 3.07 (s, 4H). $^{13}$C NMR (125.5 MHz, $CDCl_3$) δ 163.79, 148.39, 139.50, 135.44, 134.28, 133.42, 132.35, 131.26, 129.48, 128.37, 127.80, 126.41, 126.17, 126.12, 124.95, 122.36, 122.26, 121.38, 121.32, 117.68, 113.45, 46.20.

**4-((4-(1-((3-nitrophenyl)sulfonyl)-1*H*-indole-3-carbonyl)piperazin-1-yl)sulfonyl)benzonitrile (20b)**. Yield: 93.0% (purity: 99.6%); $[M+H]^+$: $C_{26}H_{22}N_5O_7S_2^+$; Calc. Mass, $[M+H]^+$: 580.1; Found mass, $[M+H]^+$: 580.05; $^1$H NMR (500 MHz, $CDCl_3$) *δ* 8.70 (s, 1H), 8.42 (d, *J* = 8.1 Hz, 1H), 8.20 (d, *J* = 7.9 Hz, 1H), 7.98 (d, *J* = 8.4 Hz,1H), 7.87 (s, 4H), 7.74 – 7.68 (m, 2H), 7.54 (d, *J* = 7.9 Hz, 1H), 7.42 (t, *J* = 7.8 Hz, 1H), 7.31 (t, *J* = 7.6 Hz, 1H), 3.80 (s, 4H), 3.10 (s, 4H). $^{13}$C NMR (125.5 MHz, $CDCl_3$) δ 163.93, 148.47, 140.15, 139.53, 134.33, 133.32, 132.40, 131.32, 128.98, 128.38, 128.31, 126.54, 126.35, 125.05, 122.32, 121.33, 117.50, 117.24, 117.19, 113.53, 46.16.

**(1-((3-nitrophenyl)sulfonyl)-1H-indol-3-yl)(4-((3-nitrophenyl)sulfonyl)piperazin-1-yl)methanone (20c)**. Yield: 84.0% (purity: 99.8%); $[M+H]^+$: $C_{25}H_{22}N_5O_9S_2^+$; Calc. Mass, $[M+H]^+$: 600.09; Found mass, $[M+H]^+$: 599.95; $^1$H NMR (500 MHz, $CDCl_3$) δ 8.71 (s, 1H),

8.59 (s, 1H), 8.50 (d, *J* = 7.3 Hz, 1H), 8.42 (d, *J* = 7.3 Hz, 1H), 8.20 (d, *J* = 7.1 Hz, 1H), 8.09 (d, *J* = 7.0 Hz, 1H), 7.98 (d, *J* = 7.9 Hz, 1H), 7.82 (t, *J* = 7.6 Hz, 1H), 7.72 (bs, 2H), 7.54 (d, *J* = 7.3 Hz, 1H), 7.44 – 7.39 (m, 1H), 7.33 – 7.29 (m, 1H), 3.82 (s, 4H), 3.14 (s, 4H). $^{13}$C NMR (125.5 MHz, $CDCl_3$) δ 163.96, 148.67, 148.47, 139.55, 138.16, 134.34, 133.21, 132.40, 131.32, 131.01, 128.99, 128.28, 127.90, 126.55, 126.42, 122.89, 122.36, 121.33, 117.49, 113.55, 46.22, 29.83.

**Computational Methods**

To obtain an appropriate model of RANKL for docking of the inhibitors, we employed the crystallographic structure of the TNF complex with SPD-304 as template.[38] The structure revealed that the small-molecule mediated displacement of one subunit of the trimer and the resulting TNF dimer retained the same subunit fold as the intact trimer. However, the angle between the two subunits was slightly widened with respect to the native trimer. The X-ray structure of the TNF complex with SPD-304 was retrieved from the Protein Data Bank (accession code 2AZ5[38]) and the protein atoms comprising chains A and B were extracted from the PDB file. A single monomer of RANKL was taken from the asymmetric unit of the recent X-ray structure of the human RANKL complex with the N-terminal fragment of its decoy receptor osteoprotegerin (PDB accession code 3URF).[19] The model of RANKL dimer was obtained by superimposing the RANKL monomer with each subunit of the TNF dimer using the multiseq module of VMD 1.9.[55] The position of hydrogen atoms were calculated using the H++ server with default parameters at pH 6.5.[56]

Atomistic molecular dynamics simulations in explicit solvent were performed with the GPU-accelerated version of PMEMD in AMBER v18,[57] using the ff14SB force field.[58] The

model of human RANKL dimer was immersed in a truncated octahedral TIP3P water box with a buffer distance of 12 Å around the solute, and then counter ions were added to neutralize the total charge of the system using the XLEaP module. Initially, energy minimization of the system was carried out with 1,000 steps of steepest descent and 1,500 steps of conjugate gradient without any restraints. Then, positional restraints of 50 $Kcal \times mol^{-1} \times Å^{-2}$ were applied to all $C^{\alpha}$ atoms, and the system was heated to 300 K within 100 ps of simulation under constant volume (NVT ensemble). The density of the system was then equilibrated under constant pressure of 1 bar and temperature of 300 K through 400 ps of simulation, in which the positional restraints were gradually removed. An additional 1,500 ps of equilibration was performed in the NPT ensemble without any restraints. Five independent production runs of 100 ns were performed in the NPT ensemble with a time step of 2 fs, using different random seed numbers for the assignment of initial velocities at 300 K. The Langevin thermostat with a collision frequency of 2 $ps^{-1}$ was used to regulate the temperature and the Berendsen weak-coupling algorithm with a relaxation time of 1 ps to regulate the pressure. The particle mesh Ewald summation method was used to treat long-range electrostatic interactions with a tolerance of $10^{-6}$. The real space cut-off was set to 9 Å and all hydrogen atoms were constrained to their equilibrium distance using the SHAKE algorithm. Trajectories were updated every 5,000 steps, resulting in 10,000 frames per 10 ps for each simulation. Analysis and clustering of the 5 trajectories was performed with the agglomerative hierarchical clustering algorithm employed in the CCPTRAJ module of AMBER.[59]

The initial conformations of the designed compounds were generated from SMILES representations using the program Omega 2.3 with default parameters.[60,61] For the

RANKL models and ligands, all non-polar hydrogen atoms were removed and Gasteiger charges were applied in AutoDockTools 1.5.4.[44] The search space was defined by a grid box centered at the interface of the RANKL dimer that comprised 80×80×60 grid points of 0.375 Å spacing. For each complex, 100 docking rounds were calculated using AutoDock 4.2, employing the Lamarckian genetic algorithm with default parameters,[62,63] except for the maximum number of energy evaluations that was set to 10 million. The resulting conformations were clustered using a 2.0-Å cutoff, while visual examination of the results and rendering of the figures was performed using PyMol 1.8.4. All calculations were carried out on an AMD workstation equipped with RTX GPUs, running under Linux 5.2 kernel with CUDA v10.

**Expression, purification and electrophoresis of human RANKL**

The extracellular domain of RANKL (Lys159 – Asp317) was expressed in BL21(DE3) pLysS strain of *E. coli* as a Glutathione S-Transferase (GST)-fusion protein as previously described.[64] GST-RANKL was purified as previously described [64] while separation of RANKL from its GST fusion partner was accomplished by proteolytic cleavage with the type-14 human rhinovirus 3C protease (America Pharmacia Biotech). The concentration of protein in the samples was determined by the Bradford method using bovine albumin as standard. Proteins were separated by electrophoresis in 12% (w/v) SDS polyacrylamide gel electrophoresis (SDS-PAGE) as previously described.[64]

**Fluorescence binding assay and determination of dissociation constant ($K_d$)**

Fluorescence intensity was measured with a Hitachi F-2500 fluorescence spectrophotometer in 1.0 x 4.5 cm quartz cuvettes at 25 ºC as previously described in [65] using the following equation:

$$F_{obs} = F_{BG} + MF_{P_F}[P_F] + FR \cdot MF_{P_F} \cdot \frac{([L_T]+[P_T]+K_d]) \pm \sqrt{([L_T]+[P_T]+K_d])^2 - 4[P_T][L_T]}}{2} \quad (1)$$

In Eq. (1) $F_{obs}$ is the observed fluorescence intensity; $F_{BG}$ is the fluorescence background signal; $MF_{P_F}$ and $P_F$ are the molar fluorescence and concentration of free protein, respectively; $FR$ is the fluorescence ratio of bound protein; $L_T$ and $P_T$ are the total concentration of ligand and protein respectively. A detailed analysis of the development of the fluorescence ligand-binding assay has been previously described.[65]

Differences in fluorescence intensity at 302 nm between the complex (RANKL/ligand) and free protein (excitation at 274 nm) were analyzed as previously described in[65] (Eq. 1) in order to determine the dissociation constant ($K_d$) of RANKL with various ligands. The experiments were performed in 25 mM Tris-HCl buffer (pH 7.5), 100 mM NaCl, containing either 5% DMSO or 5% Polyethylene glycol 3350 (PEG3350). The slits were set at 5 and 20 nm in excitation and emission respectively. In order to determine the dilution effect of RANKL (due to ligand addition) and any fluorescence effect by unbound ligand, a blank sample containing Tyr with the same fluorescence signal was titrated with ligand additions as described above. The sample absorbance was kept below 0.1 to minimize the inner filter effect.[66] Data were analyzed using Prism V.6 (GraphPad Software, San Diego, CA).

### *Ex Vivo* RANKL-induced osteoclastogenesis assay

Bone marrow (BM) cells were collected after flushing out of mouse femurs and tibiae, subjected to gradient purification using Ficoll-Paque (GE Healthcare), plated in 96-well plates at a density of 6 × $10^4$ cells per well and cultured in alpha Minimum Essential Medium (aMEM) (GIBCO) containing 10% fetal bovine serum supplemented with 40 ng/mL human RANKL prepared as previously described and 25 ng/mL macrophage colony stimulating factor (M-CSF) (R&D Systems) for 5 days.[18] All tested compounds were pre-incubated with RANKL at 5 and 10 μM in aMEM medium for 1 h at room temperature and then added to cell cultures that were replenished with fresh medium every 2 days. Osteoclasts were stained for tartrate-resistant acid phosphatase (TRAP) activity using a leukocyte acid phosphatase (TRAP kit) (Sigma–Aldrich). All animal experiments performed in the manuscript were conducted in compliance with institutional guidelines, PD 56/2013 and European Directive 2010/63/EU.

### Quantitative TRAP Activity Assay

In the TRAP activity assay, BM cells isolated as above described, were plated in 96-well plates at a density of 6 × $10^4$ cells per well and cultured in aMEM medium containing 10% fetal bovine serum supplemented with 40 ng/ml RANKL and 25 ng/ml M-CSF (R&D Systems) for 4 days. Then, cells were lysed in ice-cold phosphate buffer containing 0.1% Triton X-100. Lysates were added to 96-well plates containing phosphatase substrate (p-nitrophenol phosphate, Sigma–Aldrich) and 40 mM tartrate acid buffer and incubated at 37 ºC for 30 min. The reaction was stopped with the addition of 0.5 N NaOH. Absorbance was measured at 405 nm on a microplate reader (Optimax, Molecular Devices). TRAP activity was normalized to total protein which was determined using the Bradford assay

(Bio-Rad). Percentage of TRAP activity was calculated relatively to the absorbance of the positive control (untreated). $IC_{50}$ values (mean ± standard deviation calculated from five or more measuring points) were determined from three independent experiments.

**Phalloidin Labeling**

BM cells were seeded at 2 × $10^4$ cells/well into 24 well plates and cultured in aMEM medium (Gibco) containing 10% fetal bovine serum supplemented with 40 ng/ml RANKL and 25 ng/ml M-CSF (R&D Systems) for 4 days. All tested compounds were pre-incubated with RANKL at 5 and 10 μM in aMEM medium for 1 h at room temperature and then added to cell cultures that were replenished with fresh medium every 2 days. Cells were then fixed with 10% formalin for 10 min followed by permeabilization with 0.1% (v/v) Triton X-100 (Sigma-Aldrich). Osteoclast actin rings were stained with Alexa Fluor 488-conjugated phalloidin (Molecular Probes. Invitrogen), cells were washed PBS and stained with 4',6-diamidine-2'-phenylindole dihydrochloride (DAPI; Sigma-Aldrich). Actin rings were visualized under a fluorescence microscope Nikon and osteoclasts with intact F-actin rings were counted normalized per $mm^2$.

**Viability assay**

Cell viability was evaluated in pre-osteoclasts (bone marrow-derived macrophages, BMMs) using the 3-(4,5-dimethylthiazol-2-yl)-2,5-diphenyltetrazolium bromide (MTT) assay, which measures the ability of viable cells to reduce a soluble tetrazolium salt to an insoluble purple formazan precipitate. BM cells used for MTT assay were seeded at a density of $10^5$ cells/well in 96-well plates and incubated with all tested compounds for 48 h in aMEM containing 10% fetal bovine serum supplemented with 25 ng/ml M-CSF (R&D

Systems). After removal of the medium, each well was incubated with 0.5 mg/mL MTT (Sigma–Aldrich) in aMEM serum-free medium at 37 ºC for 2 h. At the end of the incubation period, the medium was removed and the intracellular formazan was solubilized with 200 µL DMSO and quantified by reading the absorbance at 550 nm on a microplate reader (Optimax, Molecular Devices). The percentage of cell viability was calculated based on the absorbance measured relative to the absorbance of the untreated control. $LC_{50}$ values (mean ± standard deviation calculated from five or more measuring points) were determined from three independent experiments.

**Cross-Linking Assay and SDS-PAGE**

The chemical crosslinking reagent disuccinimidyl suberate (DSS) (Sigma–Aldrich) was used to examine the RANKL conformation as trimers, dimers, and monomers. 50 mM of DSS was prepared as a stock solution in dimethyl sulfoxide. All tested compounds were preincubated either at an equal molar ratio or excess with human RANKL for 1 h at room temperature and then crosslinked with 1 mM DSS. The crosslinking reactions were carried out for 1 h at room temperature and terminated with 50 mM Tris (pH 7.5) for 30 min. The crosslinked complex was separated in a 12% sodium dodecyl sulfate-polyacrylamide gel electrophoresis (SDS-PAGE) and immunoblotted using a polyclonal human RANKL antibody (R&D Systems). Western blots have been repeated at least twice for each compound.

**Western Blotting for NFATc1 and c-Fos**

RAW264.7 cells were plated in 48-well plates at a density of 6 × $10^4$ cells per well and cultured in aMEM medium containing 10% fetal bovine serum supplemented with 40 ng/mL RANKL (R&D Systems). All tested compounds were pre-incubated with RANKL at 2, 5, and 10 μM in aMEM medium for 1 h at room temperature and then added to cell cultures for 2 days. RAW264.7 whole cell lysates were isolated, separated by SDS-PAGE, and transferred onto nitrocellulose membranes (Millipore, Bedford, MA, U.S.A.). The membranes were blocked with 5% BSA fraction V in PBS-T (PBS, 0.1% Tween 20), and immunostained with polyclonal antibodies against NFATc1 (Proteintech), c-Fos (SantaCruz Biotechnology) and actin (Santa Cruz Biotechnology). The intensities of NFATc1 and c-Fos protein bands were analyzed and normalized against actin protein band (ImageLab Software, Biorad). Western blots have been repeated at least twice for each compound.

**MC3T3-E1 differentiation and ALP activity**

The mouse pre-osteoblastic cell line MC3T3-E1 (ATCC, USA), was maintained in aMEM medium (Gibco) with 10% FBS in the absence of ascorbic acid. The cells were cultured at 37 ºC in a humid atmosphere containing 5% $CO_2$. For the osteoblast differentiation determination, the cells were seeded at a density of 2.5×$10^4$ cells/well in a 24-well plate, and cultured in aMEM containing 10% fetal bovine serum, 2 mM L-glutamate, 10 mM β-glycerol phosphate (Sigma-Aldrich), 50 μg/mL ascorbic acid (Sigma-Aldrich) and all tested compounds were added at concentrations of 2, 5 and 10 μM for 14 days. Cell culture media were changed every 3 days. ALP activity was determined using p-nitrophenyl phosphate substrate (p-NPP). On day 14, cells were washed with cold PBS

and lysed with saline and 1% NP40. Then cell lysate was mixed with 100 µL of 6.7mmol/L p-nitrophenyl phosphate solution (Sigma–Aldrich) and incubated at 37 °C for 1h. Absorbance was measured at 405 nm on a microplate reader (Optimax, Molecular Devices). ALP activity was normalized to total protein which was determined using the Bradford assay (Bio-Rad). ALP Activity/µg of total protein is expressed as a percentage of the positive control.

**Statistical Analysis**

All results are expressed as mean ± standard deviation (SD). Statistical significance was calculated for two groups using Student's t-tests. One-Way analysis of variance (ANOVA) and Tukey post-hoc test was performed to compare means of multiple groups. P-values <0.05 were considered significant; *$p < 0.05$, **$p < 0.01$, ***$p < 0.001$ when not otherwise specified.

## ASSOCIATED CONTENT

### Supporting information

The supporting information is available free of charge via the Internet at http://pubs.acs.org

Detailed computation results; additional biological results; $^{1}H$ and $^{13}C$ NMR data and LC-MS analysis of all new compounds (PDF)

Molecular Formula Strings of all compounds tested (CSV)

Selected physiochemical descriptors of the compounds computed using SwissADME server (XLSX)

Coordinates for the initial, energy minimized model of human RANKL dimer employed in the calculations (PDB).

## AUTHOR INFORMATION

### Corresponding Author

*E-mail: douni@aua.gr

### ORCID

Eleni Douni: 0000-0003-0004-5121

### Author contributions

The manuscript was written with contributions from all authors. All authors have given approval to the final version of the manuscript.

## Notes

The authors declare no competing financial interest.

## ACKNOWLEDGMENTS

This work was funded by the project TheRAlead (09SYN-21-784) co-financed by the European Union (European Regional Development Fund-ERDF) and Greek national funds through the Operational Program "Competitiveness & Entrepreneurship", NSRF 2007-2013 in the context of GSRT-National action "Cooperation".

## ABBREVIATIONS USED

ALP, alkaline phosphatase; aMEM, alpha Minimum Essential Medium; BM, Bone marrow; BMMs, bone marrow-derived macrophages; DAPI, 4',6-diamidine-2'-phenylindole dihydrochloride; DMSO, Dimethyl sulfoxide; DSS, disuccinimidyl suberate; $IC_{50}$, half maximal inhibitory concentration; $K_d$, dissociation constant; $LC_{50}$, 50% lethal concentration; M-CSF, macrophage colony stimulating factor; MTT, 3-(4,5-dimethylthiazol-2-yl)-2,5-diphenyltetrazolium bromide; NFATc1, nuclear factor of activated T-cell c1; NF-κB, nuclear factor κB; OPG, osteoprotegerin; RANKL, Receptor activator of nuclear factor-κB ligand; SDS-PAGE, sodium dodecyl sulfate-polyacrylamide gel electrophoresis; TNF, tumor necrosis factor; TRAP, tartrate-resistant acid phosphatase.

## REFERENCES


(1) Gullberg, B.; Johnell, O.; Kanis, J. A. World-Wide Projections for Hip Fracture. *Osteoporos. Int.* **1997**, *7* (5), 407–413.

(2) Lacey, D. L.; Tan, H. L.; Lu, J.; Kaufman, S.; Van, G.; Qiu, W.; Rattan, A.; Scully, S.; Fletcher, F.; Juan, T.; Kelley, M.; Burgess, T. L.; Boyle, W. J.; Polverino, A. J. Osteoprotegerin Ligand Modulates Murine Osteoclast Survival in Vitro and in Vivo. *Am. J. Pathol.* **2000**, *157* (2), 435–448.

(3) Lacey, D. L.; Timms, E.; Tan, H. L.; Kelley, M. J.; Dunstan, C. R.; Burgess, T.; Elliott, R.; Colombero, A.; Elliott, G.; Scully, S.; Hsu, H.; Sullivan, J.; Hawkins, N.; Davy, E.; Capparelli, C.; Eli, A.; Qian, Y. X.; Kaufman, S.; Sarosi, I.; Shalhoub, V.; Senaldi, G.; Guo, J.; Delaney, J.; Boyle, W. J. Osteoprotegerin Ligand Is a Cytokine That Regulates Osteoclast Differentiation and Activation. *Cell* **1998**, *93* (2), 165–176.

(4) Fuller, K.; Wong, B.; Fox, S.; Choi, Y.; Chambers, T. J. TRANCE Is Necessary and Sufficient for Osteoblast-Mediated Activation of Bone Resorption in Osteoclasts. *J. Exp. Med.* **1998**, *188* (5), 997–1001.

(5) Ito, S.; Wakabayashi, K.; Ubukata, O.; Hayashi, S.; Okada, F.; Hata, T. Crystal Structure of the Extracellular Domain of Mouse RANK Ligand at 2.2-A Resolution. *J. Biol. Chem.* **2002**, *277* (8), 6631–6636.

(6) Lam, J.; Nelson, C. A.; Ross, F. P.; Teitelbaum, S. L.; Fremont, D. H. Crystal Structure of the TRANCE/RANKL Cytokine Reveals Determinants of Receptor-Ligand Specificity. *J. Clin. Invest.* **2001**, *108* (7), 971–979.

(7) Ikeda, T.; Kasai, M.; Utsuyama, M.; Hirokawa, K. Determination of Three Isoforms of the Receptor Activator of Nuclear Factor-KappaB Ligand and Their Differential Expression in Bone and Thymus. *Endocrinology* **2001**, *142* (4), 1419–1426.

(8) Hikita, A.; Yana, I.; Wakeyama, H.; Nakamura, M.; Kadono, Y.; Oshima, Y.; Nakamura, K.; Seiki, M.; Tanaka, S. Negative Regulation of Osteoclastogenesis by Ectodomain Shedding of Receptor Activator of NF-KB Ligand. *J. Biol. Chem.* **2006**, *281* (48), 36846–36855.

(9) Liu, C.; Walter, T. S.; Huang, P.; Zhang, S.; Zhu, X.; Wu, Y.; Wedderburn, L. R.; Tang, P.; Owens, R. J.; Stuart, D. I.; Ren, J.; Gao, B. Structural and Functional Insights of RANKL-RANK Interaction and Signaling. *J. Immunol.* **2010**, *184* (12), 6910–6919.

(10) Takayanagi, H. Osteoimmunology: Shared Mechanisms and Crosstalk between the Immune and Bone Systems. *Nat. Rev. Immunol.* **2007**, *7* (4), 292–304.

(11) Hanada, R.; Leibbrandt, A.; Hanada, T.; Kitaoka, S.; Furuyashiki, T.; Fujihara, H.; Trichereau, J.; Paolino, M.; Qadri, F.; Plehm, R.; Klaere, S.; Komnenovic, V.; Mimata, H.; Yoshimatsu, H.; Takahashi, N.; von Haeseler, A.; Bader, M.; Kilic, S. S.; Ueta, Y.; Pifl, C.; Narumiya, S.; Penninger, J. M. Central Control of Fever and

Female Body Temperature by RANKL/RANK. *Nature* **2009**, *462* (7272), 505–509.

(12) Fata, J. E.; Kong, Y. Y.; Li, J.; Sasaki, T.; Irie-Sasaki, J.; Moorehead, R. A.; Elliott, R.; Scully, S.; Voura, E. B.; Lacey, D. L.; Boyle, W. J.; Khokha, R.; Penninger, J. M. The Osteoclast Differentiation Factor Osteoprotegerin-Ligand Is Essential for Mammary Gland Development. *Cell* **2000**, *103* (1), 41–50.

(13) Schramek, D.; Leibbrandt, A.; Sigl, V.; Kenner, L.; Pospisilik, J. A.; Lee, H. J.; Hanada, R.; Joshi, P. A.; Aliprantis, A.; Glimcher, L.; Pasparakis, M.; Khokha, R.; Ormandy, C. J.; Widschwendter, M.; Schett, G.; Penninger, J. M. Osteoclast Differentiation Factor RANKL Controls Development of Progestin-Driven Mammary Cancer. *Nature* **2010**, *468* (7320), 98–102.

(14) Kong, Y. Y.; Yoshida, H.; Sarosi, I.; Tan, H. L.; Timms, E.; Capparelli, C.; Morony, S.; Oliveira-dos-Santos, a J.; Van, G.; Itie, a; Khoo, W.; Wakeham, a; Dunstan, C. R.; Lacey, D. L.; Mak, T. W.; Boyle, W. J.; Penninger, J. M. OPGL Is a Key Regulator of Osteoclastogenesis, Lymphocyte Development and Lymph-Node Organogenesis. *Nature* **1999**, *397* (6717), 315–323.

(15) Dougall, W. C.; Glaccum, M.; Charrier, K.; Rohrbach, K.; Brasel, K.; De Smedt, T.; Daro, E.; Smith, J.; Tometsko, M. E.; Maliszewski, C. R.; Armstrong, A.; Shen, V.; Bain, S.; Cosman, D.; Anderson, D.; Morrissey, P. J.; Peschon, J. J.; Schuh, J. A. RANK Is Essential for Osteoclast and Lymph Node Development. *Genes Dev.* **1999**, *13* (18), 2412–2424.

(16) Kim, N.; Odgren, P. R.; Kim, D. K.; Marks, S. C.; Choi, Y. Diverse Roles of the Tumor Necrosis Factor Family Member TRANCE in Skeletal Physiology Revealed by TRANCE Deficiency and Partial Rescue by a Lymphocyte-Expressed TRANCE Transgene. *Proc. Natl. Acad. Sci. U. S. A.* **2000**, *97* (20), 10905–10910.

(17) Li, J.; Sarosi, I.; Yan, X. Q.; Morony, S.; Capparelli, C.; Tan, H. L.; McCabe, S.; Elliott, R.; Scully, S.; Van, G.; Kaufman, S.; Juan, S. C.; Sun, Y.; Tarpley, J.; Martin, L.; Christensen, K.; McCabe, J.; Kostenuik, P.; Hsu, H.; Fletcher, F.; Dunstan, C. R.; Lacey, D. L.; Boyle, W. J. RANK Is the Intrinsic Hematopoietic Cell Surface Receptor That Controls Osteoclastogenesis and Regulation of Bone Mass and Calcium Metabolism. *Proc. Natl. Acad. Sci. U. S. A.* **2000**, *97* (4), 1566–1571.

(18) Douni, E.; Rinotas, V.; Makrinou, E.; Zwerina, J.; Penninger, J. M.; Eliopoulos, E.; Schett, G.; Kollias, G. A RANKL G278R Mutation Causing Osteopetrosis Identifies a Functional Amino Acid Essential for Trimer Assembly in RANKL and TNF. *Hum. Mol. Genet.* **2012**, *21* (4), 784–798.

(19) Luan, X.; Lu, Q.; Jiang, Y.; Zhang, S.; Wang, Q.; Yuan, H.; Zhao, W.; Wang, J.; Wang, X. Crystal Structure of Human RANKL Complexed with Its Decoy Receptor Osteoprotegerin. *J. Immunol.* **2012**, *189* (1), 245–252.

(20) Sezer, O.; Heider, U.; Zavrski, I.; Kühne, C. A.; Hofbauer, L. C. RANK Ligand and Osteoprotegerin in Myeloma Bone Disease. *Blood* **2003**, *101* (6), 2094–2098.

(21) Sisay, M.; Mengistu, G.; Edessa, D. The RANK/RANKL/OPG System in

Tumorigenesis and Metastasis of Cancer Stem Cell: Potential Targets for Anticancer Therapy. *Onco. Targets. Ther.* **2017**, *10*, 3801–3810.

(22) Rinotas, V.; Niti, A.; Dacquin, R.; Bonnet, N.; Stolina, M.; Han, C.-Y.; Kostenuik, P.; Jurdic, P.; Ferrari, S.; Douni, E. Novel Genetic Models of Osteoporosis by Overexpression of Human RANKL in Transgenic Mice. *J. Bone Miner. Res.* **2014**, *29* (5), 1158–1169.

(23) Crockett Julie, D. S. Osteoporosis – a Current View of Pharmacological Prevention and Treatment. *Drug Des. Dev. Ter.* **2013**, *7*, 435–448.

(24) Kong Wah, N.; Martin, T. J. New Therapeutics for Osteoporosis. *Curr. Opin. Pharmacol.* **2014**, *16C*, 58–63.

(25) Rizzoli, R.; Reginster, J.-Y. Adverse Drug Reactions to Osteoporosis Treatments. *Expert Rev. Clin. Pharmacol.* **2011**, *4* (5), 593–604.

(26) Kostenuik, P. J.; Nguyen, H. Q.; Mccabe, J.; Warmington, K. S.; Kurahara, C.; Sun, N.; Chen, C.; Li, L.; Cattley, R. C.; Van, G.; Scully, S.; Elliott, R.; Grisanti, M.; Morony, S.; Tan, H. L.; Asuncion, F.; Li, X.; Ominsky, M. S.; Stolina, M.; Dwyer, D.; Dougall, W. C.; Hawkins, N.; Boyle, W. J.; Simonet, W. S.; Sullivan, J. K. Denosumab, a Fully Human Monoclonal Antibody to RANKL, Inhibits Bone Resorption and Increases BMD in Knock-In Mice That Express Chimeric (Murine/Human) RANKL*. *J. Bone Miner. Res.* **2009**, *24* (2), 182–195.

(27) Stopeck, A. T.; Lipton, A.; Body, J. J.; Steger, G. G.; Tonkin, K.; De Boer, R. H.; Lichinitser, M.; Fujiwara, Y.; Yardley, D. A.; Viniegra, M.; Fan, M.; Jiang, Q.; Dansey, R.; Jun, S.; Braun, A. Denosumab Compared with Zoledronic Acid for the Treatment of Bone Metastases in Patients with Advanced Breast Cancer: A Randomized, Double-Blind Study. *J. Clin. Oncol.* **2010**, *28* (35), 5132–5139.

(28) Watts, N. B.; Brown, J. P.; Papapoulos, S.; Lewiecki, E. M.; Kendler, D. L.; Dakin, P.; Wagman, R. B.; Wang, A.; Daizadeh, N. S.; Smith, S.; Bone, H. G. Safety Observations With 3 Years of Denosumab Exposure: Comparison Between Subjects Who Received Denosumab During the Randomized FREEDOM Trial and Subjects Who Crossed Over to Denosumab During the FREEDOM Extension. *J. Bone Miner. Res.* **2017**, *32* (7), 1481–1485.

(29) Chames, P.; Van Regenmortel, M.; Weiss, E.; Baty, D. Therapeutic Antibodies: Successes, Limitations and Hopes for the Future. *Br. J. Pharmacol.* **2009**, *157* (2), 220–233.

(30) Cheng, X.; Kinosaki, M.; Takami, M.; Choi, Y.; Zhang, H.; Murali, R. Disabling of Receptor Activator of Nuclear Factor-KB (RANK) Receptor Complex by Novel Osteoprotegerin-like Peptidomimetics Restores Bone Loss in Vivo. *J. Biol. Chem.* **2004**, *279* (9), 8269–8277.

(31) Ta, H. M.; Nguyen, G. T. T.; Jin, H. M.; Choi, J.; Park, H.; Kim, N.; Hwang, H.-Y.; Kim, K. K. Structure-Based Development of a Receptor Activator of Nuclear Factor-B Ligand (RANKL) Inhibitor Peptide and Molecular Basis for Osteopetrosis. *Proc.*

*Natl. Acad. Sci.* **2010**, *107* (47), 20281–20286.

(32) Melagraki, G.; Ntougkos, E.; Papadopoulou, D.; Rinotas, V.; Leonis, G.; Douni, E.; Afantitis, A.; Kollias, G. In Silico Discovery of Plant-Origin Natural Product Inhibitors of Tumor Necrosis Factor (TNF) and Receptor Activator of NF-KB Ligand (RANKL). *Front. Pharmacol.* **2018**, *9*, 800.

(33) Zhu, M.; Kim, M. H.; Lee, S.; Bae, S. J.; Kim, S. H.; Park, S. B. Discovery of Novel Benzopyranyl Tetracycles That Act as Inhibitors of Osteoclastogenesis Induced by Receptor Activator of NF-KB Ligand. *J. Med. Chem.* **2010**, *53* (24), 8760–8764.

(34) Tseng, C.-H.; Lin, R.-W.; Chen, Y.-L.; Wang, G.-J.; Ho, M.-L.; Tzeng, C.-C. Discovery of Indeno[1,2-c]Quinoline Derivatives as Inhibitors of Osteoclastogenesis Induced by Receptor Activator of NF-KB Ligand (RANKL). *J. Med. Chem.* **2011**, *54* (8), 3103–3107.

(35) Chen, C.-L.; Liu, F.-L.; Lee, C.-C.; Chen, T.-C.; Ahmed Ali, A. A.; Sytwu, H.-K.; Chang, D.-M.; Huang, H.-S. Modified Salicylanilide and 3-Phenyl-2H-Benzo[e][1,3]Oxazine-2,4(3H)-Dione Derivatives as Novel Inhibitors of Osteoclast Differentiation and Bone Resorption. *J. Med. Chem.* **2014**, *57* (19), 8072–8085.

(36) Melagraki, G.; Ntougkos, E.; Rinotas, V.; Papaneophytou, C.; Leonis, G.; Mavromoustakos, T.; Kontopidis, G.; Douni, E.; Afantitis, A.; Kollias, G. Cheminformatics-Aided Discovery of Small-Molecule Protein-Protein Interaction (PPI) Dual Inhibitors of Tumor Necrosis Factor (TNF) and Receptor Activator of NF-KB Ligand (RANKL). *PLoS Comput. Biol.* **2017**, *13* (4), e1005372.

(37) Jiang, M.; Peng, L.; Yang, K.; Wang, T.; Yan, X.; Jiang, T.; Xu, J.; Qi, J.; Zhou, H.; Qian, N.; Zhou, Q.; Chen, B.; Xu, X.; Deng, L.; Yang, C. Development of Small-Molecules Targeting Receptor Activator of Nuclear Factor-KB Ligand (RANKL)—Receptor Activator of Nuclear Factor-KB (RANK) Protein–Protein Interaction by Structure-Based Virtual Screening and Hit Optimization. *J. Med. Chem.* **2019**, *62* (11), 5370–5381.

(38) He, M. M.; Smith, A. S.; Oslob, J. D.; Flanagan, W. M.; Braisted, A. C.; Whitty, A.; Cancilla, M. T.; Wang, J.; Lugovskoy, A. a; Yoburn, J. C.; Fung, A. D.; Farrington, G.; Eldredge, J. K.; Day, E. S.; Cruz, L. a; Cachero, T. G.; Miller, S. K.; Friedman, J. E.; Choong, I. C.; Cunningham, B. C. Small-Molecule Inhibition of TNF-Alpha. *Science* **2005**, *310* (5750), 1022–1025.

(39) Skiles, G. L.; Yost, G. S. Mechanistic Studies on the Cytochrome P450-Catalyzed Dehydrogenation of 3-Methylindole. *Chem. Res. Toxicol.* **1996**, *9* (1), 291–297.

(40) Sun, H.; Yost, G. S. Metabolic Activation of a Novel 3-Substituted Indole-Containing TNF-α Inhibitor: Dehydrogenation and Inactivation of CYP3A4. *Chem. Res. Toxicol.* **2008**, *21* (2), 374–385.

(41) Alexiou, P.; Papakyriakou, A.; Ntougkos, E.; Papaneophytou, C. P.; Liepouri, F.; Mettou, A.; Katsoulis, I.; Maranti, A.; Tsiliouka, K.; Strongilos, A.; Chaitidou, S.; Douni, E.; Kontopidis, G.; Kollias, G.; Couladouros, E.; Eliopoulos, E. Rationally

Designed Less Toxic SPD-304 Analogs and Preliminary Evaluation of Their TNF Inhibitory Effects. *Arch. Pharm. (Weinheim).* **2014**, *347* (11), 798–805.

(42) Papaneophytou, C.; Alexiou, P.; Papakyriakou, A.; Ntougkos, E.; Tsiliouka, K.; Maranti, A.; Liepouri, F.; Strongilos, A.; Mettou, A.; Couladouros, E.; Eliopoulos, E.; Douni, E.; Kollias, G.; Kontopidis, G. Synthesis and Biological Evaluation of Potential Small Molecule Inhibitors of Tumor Necrosis Factor. *Medchemcomm* **2015**, *6* (6), 1196–1209.

(43) Muller, P. Y.; Milton, M. N. The Determination and Interpretation of the Therapeutic Index in Drug Development. *Nat. Rev. Drug Discov.* **2012**, *11* (10), 751–761.

(44) Morris, G. M.; Huey, R.; Lindstrom, W.; Sanner, M. F.; Belew, R. K.; Goodsell, D. S.; Olson, A. J. AutoDock4 and AutoDockTools4: Automated Docking with Selective Receptor Flexibility. *J Comp Chem* **2009**, *30* (16), 2785–2791.

(45) Huang, S. Y.; Zou, X. Ensemble Docking of Multiple Protein Structures: Considering Protein Structural Variations in Molecular Docking. *Proteins Struct. Funct. Genet.* **2007**, *66* (2), 399–421.

(46) Amaro, R. E.; Baudry, J.; Chodera, J.; Demir, Ö.; McCammon, J. A.; Miao, Y.; Smith, J. C. Ensemble Docking in Drug Discovery. *Biophys. J.* **2018**, *114* (10), 2271–2278.

(47) Cosconati, S.; Forli, S.; Perryman, A. L.; Harris, R.; Goodsell, D. S.; Olson, A. J. Virtual Screening with AutoDock: Theory and Practice. *Expert Opin. Drug Discov.* **2010**, *5* (6), 597–607.

(48) Kozakov, D.; Hall, D. R.; Xia, B.; Porter, K. A.; Padhorny, D.; Yueh, C.; Beglov, D.; Vajda, S. The ClusPro Web Server for Protein-Protein Docking. *Nat. Protoc.* **2017**, *12* (2), 255–278.

(49) Asagiri, M.; Takayanagi, H. The Molecular Understanding of Osteoclast Differentiation. *Bone* **2007**, *40* (2), 251–264.

(50) Takayanagi, H.; Kim, S.; Koga, T.; Nishina, H.; Isshiki, M.; Yoshida, H.; Saiura, A.; Isobe, M.; Yokochi, T.; Inoue, J.; Wagner, E. F.; Mak, T. W.; Kodama, T.; Taniguchi, T. Induction and Activation of the Transcription Factor NFATc1 (NFAT2) Integrate RANKL Signaling in Terminal Differentiation of Osteoclasts. *Dev. Cell* **2002**, *3* (6), 889–901.

(51) Bishop, K. a; Coy, H. M.; Nerenz, R. D.; Meyer, M. B.; Pike, J. W. Mouse Rankl Expression Is Regulated in T Cells by C-Fos through a Cluster of Distal Regulatory Enhancers Designated the T Cell Control Region. *J. Biol. Chem.* **2011**, *286* (23), 20880–20891.

(52) Nepali, K.; Lee, H. Y.; Liou, J. P. Nitro-Group-Containing Drugs. *J. Med. Chem.* **2019**, *62* (6), 2851–2893.

(53) Lee, C. C.; Liu, F. L.; Chen, C. L.; Chen, T. C.; Chang, D. M.; Huang, H. S. Discovery of 5-(2′,4′-Difluorophenyl)-Salicylanilides as New Inhibitors of Receptor

Activator of NF-K°B Ligand (RANKL)-Induced Osteoclastogenesis. *Eur. J. Med. Chem.* **2015**, *98*, 115–126.

(54) Pativada, T.; Kim, M. H.; Lee, J. H.; Hong, S. S.; Choi, C. W.; Choi, Y. H.; Kim, W. J.; Song, D. W.; Park, S. I.; Lee, E. J.; Seo, B. Y.; Kim, H.; Kim, H. K.; Lee, K. H.; Ahn, S. K.; Ku, J. M.; Park, G. H. Benzylideneacetone Derivatives Inhibit Osteoclastogenesis and Activate Osteoblastogenesis Independently Based on Specific Structure-Activity Relationship. *J. Med. Chem.* **2019**, *62* (13), 6063–6082.

(55) Humphrey W.; Dalke A.; Schulten K. VMD: Visual Molecular Dynamics. *J. Mol. Graph.* **1996**, *14* (1), 33–38.

(56) Anandakrishnan, R.; Aguilar, B.; Onufriev, A. H++ 3.0: Automating PK Prediction and the Preparation of Biomolecular Structures for Atomistic Molecular Modeling and Simulations - PubMed. *Nucleic Acids Res.* **2012**, *40*, W537–W541.

(57) Salomon-Ferrer, R.; Götz, A. W.; Poole, D.; Le Grand, S.; Walker, R. C. Routine Microsecond Molecular Dynamics Simulations with AMBER on GPUs. 2. Explicit Solvent Particle Mesh Ewald. *J. Chem. Theory Comput.* **2013**, *9* (9), 3878–3888.

(58) Maier, J. A.; Martinez, C.; Kasavajhala, K.; Wickstrom, L.; Hauser, K. E.; Simmerling, C. Ff14SB: Improving the Accuracy of Protein Side Chain and Backbone Parameters from Ff99SB. *J. Chem. Theory Comput.* **2015**, *11* (8), 3696–3713.

(59) Roe, D. R.; Cheatham, T. E. PTRAJ and CPPTRAJ: Software for Processing and Analysis of Molecular Dynamics Trajectory Data. *J. Chem. Theory Comput.* **2013**, *9* (7), 3084–3095.

(60) OMEGA 3.1.2.2: OpenEye Scientific Software, Santa Fe, NM. *http://www.eyesopen.com*.

(61) Hawkins, P. C. D.; Skillman, A. G.; Warren, G. L.; Ellingson, B. A.; Stahl, M. T. Conformer Generation with OMEGA: Algorithm and Validation Using High Quality Structures from the Protein Databank and Cambridge Structural Database. *J. Chem. Inf. Model.* **2010**, *50* (4), 572–584.

(62) Morris, G. M.; Goodsell, D. S.; Halliday, R. S.; Huey, R.; Hart, W. E.; Belew, R. K.; Olson, A. J. Automated Docking Using a Lamarckian Genetic Algorithm and an Empirical Binding Free Energy Function. *J. Comput. Chem.* **1998**, *19* (14), 1639–1662.

(63) Huey, R.; Morris, G. M.; Olson, A. J.; Goodsell, D. S. A Semiempirical Free Energy Force Field with Charge-Based Desolvation. *J. Comput. Chem.* **2007**, *28* (6), 1145–1152.

(64) Papaneophytou, C. P.; Rinotas, V.; Douni, E.; Kontopidis, G. A Statistical Approach for Optimization of RANKL Overexpression in Escherichia Coli: Purification and Characterization of the Protein. *Protein Expr. Purif.* **2013**, *90* (1), 9–19.

(65) Papaneophytou, C. P.; Mettou, A. K.; Rinotas, V.; Douni, E.; Kontopidis, G. A.

Solvent Selection for Insoluble Ligands, a Challenge for Biological Assay Development: A TNF-α/SPD304 Study. *ACS Med. Chem. Lett.* **2013**, *4* (1), 137–141.

(66) Lakowicz, J. R. *Principles of Fluorescence Spectroscopy*; 3rd Edition, Springer, New York, 2006.

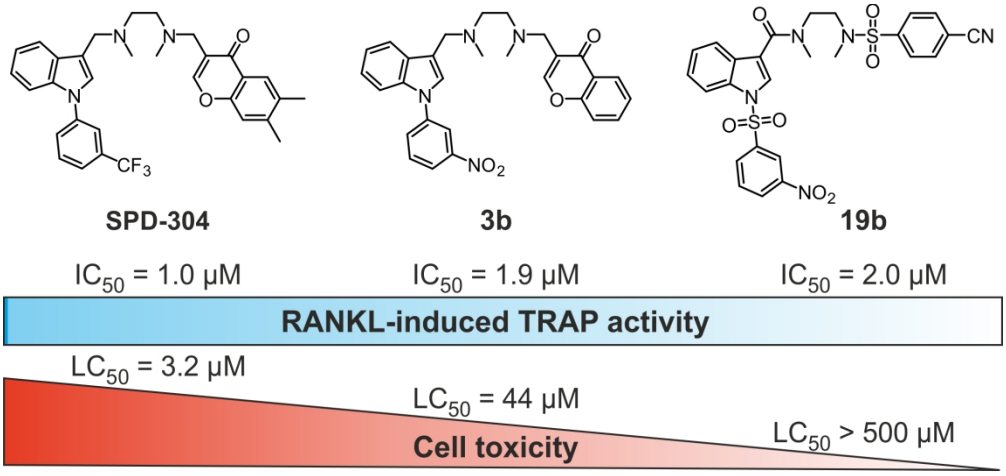
SPD-304
3b
19b
IC50 = 1.0 μM
IC50 = 1.9 μM
IC50 = 2.0 μM
RANKL-induced TRAP activity
LC50 = 3.2 μM
LC50 = 44 μM
LC50 > 500 μM
Cell toxicity

TOC